

The Specialist Committee on *Esso Osaka*

Final Report and Recommendations to the 23rd ITTC

1. GENERAL

1.1. Membership and meetings

The Specialist Committee on *Esso Osaka* was organized by five members and five meetings were held.

The membership was

Prof. H. Kobayashi, Japan (Chairman)

Dr. J.J. Blok, Netherlands (Secretary)

Dr. R. Barr, USA

Dr. Y. S. Kim, Korea

Dr. J. Nowicki, Poland

Committee meetings were held five times in the three years since last conference as shown below,

1st July 2000 Boston, USA

2nd Nov. 2000 Wageningen, Netherlands

3rd May 2001 Ilawa, Poland

4th Oct. 2001 Tokyo, Japan

5th Feb. 2002 Taejon, Korea

1.2. Task proposed by 22nd ITTC

The studies on the *Esso Osaka* were carried out in Maneuvering Committee in 21st ITTC. As a result of studies, following issues are proposed to continue the analysis of the

Esso Osaka data in the following areas and to organize a workshop to present the *Esso Osaka* benchmark data and the results of the analysis:

- a) Reduce the scatter in existing data either by eliminating suspect data sets, or by stimulating new, benchmark quality experiments.
- b) Compare propeller and rudder forces and propeller-hull-rudder interactions.
- c) Carry out a systematic series of simulations using one reference mathematical model (e.g. MMG with fixed propeller and rudder forces and interactions) using available sets of hull damping coefficients (linear and nonlinear).
- d) Compare the results of these systematic simulations with available track data and particularly the full scale trials data.

1.3. Use of *Esso Osaka* trial data as benchmark

At the first meeting of the Maneuvering Committee of the 21st ITTC in Trondheim, Norway, the Committee selected an ITTC benchmark ship for comparison of various methods for predicting ship maneuverability. Ships considered as this benchmark were the *Mariner*, which was extensively investigated by the Maneuvering Committee of the 11th and 12th ITTC, the *Esso Osaka* for which un-

usually complete trials results and model test data were available, Crane (1979a) and Barr (1993), and a more modern ship form, such as one of the MARAD Series Models described by Roseman (1987). The *Esso Osaka* was selected for the reasons noted in the following sections.

The primary advantages of *Esso Osaka* trials data as a maneuvering benchmark were:

1. An unusually extensive set of trials of the *Esso Osaka* at full load draft had been conducted with unusual attention to measurement accuracy, including correction of trials results for the effects of ocean current measured during the trials, Crane (1979a, 1979b).
2. Conduct of trials in deep water and in water depths equal to 1.5 and 1.2 times trials draft.
3. Captive model tests or free running model tests of the *Esso Osaka* had been carried out by at least 20 different laboratories, using models with lengths ranging from 1.65 to 8.125 meters.
4. Drawings of the *Esso Osaka* hull, propeller and rudder, required for the RANS calculations planned by the Maneuvering Committee, had been made available by EXXON.

In addition, a significant body of *Esso Osaka* captive model test data had been previously collected for a USA Marine Board study of ship maneuvering simulators and simulation, Webster (1992), and an analysis of those data for that study had been reported by Barr (1993).

The primary disadvantages of the *Esso Osaka* as a maneuverability benchmark were:

1. The relative old hull form of a ship launched in 1973.
2. The conduct of the benchmark trials before the availability of shipboard GPS and the improved tracking accuracy available

with GPS.

3. The unavailability of good quality resistance or propulsion data, which would also allow use of the *Esso Osaka* as a benchmark for RANS flow calculations or other ITTC studies.

Data for the *Mariner* were rejected as a benchmark, despite the availability of extensive trials data and model test data because maneuverability of that ship had already been studied by ITTC Committees and because the *Mariner* was an old and very atypical hull form, and only four ships of the class were ever built. No other comprehensive source of ship and model test data for any ships of more “modern” hull form could be identified by the Committee.

The shortcomings of the *Esso Osaka* data were considered minor when compared with their advantages, and the Maneuvering Committee selected the *Esso Osaka* as its benchmark. The number of Ocean Engineering topics and Procedures should be continuously maintained. A practical solution should be found.

1.4. Lines on studies in *Esso Osaka* Specialist Committee

In first stage of this study, proposed data which were discussed in Maneuvering committee in 22nd ITTC were examined to know the detail experimental conditions and analyzing procedures. It was confirmed that there are mainly two kinds of mathematical models for expression of ship maneuvering motion. The proposed data may be different relating to the mathematical model that is used for expression of motion. Two mathematical models are selected to discuss the hydrodynamic coefficients and interaction forces. One of them is MMG model (MMG, 1985), the other is whole ship model: WSM. The details of the models are explained in chapter 5 and chapter 6.

In chapter 3 in this report, the reasons of scatter in proposed data sets are discussed. There are many kinds of reason which occur the scattering in measured hydrodynamic forces and the coefficients. Therefore, in order to discuss the benchmark data, the data of which we can know the experimental conditions and analyzing procedures should be chosen.

In chapter 2, the discussion on proposed data in 21st ITTC and the scattering are analyzed. The potential reasons of scattering of hydrodynamic coefficients shown in proposed data are discussed in chapter 3. In chapter 4, the proposed test data including full scale trial tests and free running model tests are summarized. These results are target data of simulation using estimated hydrodynamic forces. The discussion in chapter 5 and chapter 6 are main parts of this report. The contents of proposed data are studied for estimation of maneuvering motion of *Esso Osaka*. The discussions on proposed data are studied based on MMG model and Whole ship model. Finally, Benchmark data on hull and propeller and rudder interaction are proposed in conclusion.

2. A COMPARISON OF MEASURED DAMPING FORCES

2.1. Sources of hydrodynamic data

Force data for the *Esso Osaka* were available primarily in the form of hydrodynamic coefficients derived from captive model test data. Raw data or published plots of measured forces versus test variables were available for only a few tests, and the widely varying drift angle and yaw rates of the tests made a meaningful comparisons of the force data problematic. 20 sets of hydrodynamic coefficients for the *Esso Osaka* obtained by 18 laboratories were collected and analyzed by the 22nd ITTC Maneuvering Committee. The present Committee has obtained four additional sets of test data relating to WSM from laboratories

in Korea. The present Committee also decided to eliminate from further consideration four of the earlier data sets which were judged for various reasons to be not reliable. As most data were understood to have been obtained using models with rudder installed, only those data were considered. A total of 15 data sets were therefore considered in order to investigate the scattering of predicted damping forces and moments.

2.2. Summary of data comparisons

Predicted sway damping forces and yaw damping moments were compared for data sets understood to be for tests with rudder installed. In many cases the data source did not indicate the operating condition of the propeller, or in some cases even if one was installed. It was assumed that all data were obtained with a propeller operating at either model or ship self propulsion point.

Total damping forces and moments were calculated for combination of five steady drift angle, $\beta = \sin^{-1}(v/U)$ and six non-dimensional yaw rate, $r' = rL/U$. Figures 2.1 and 2.2 compare typical results for an eight degree drift angle, for tests where a rudder was known or believed to be installed. These figures show rather large variations in total forces and moments, although the scatter is not as large as that found by the 22nd ITTC Maneuvering Committee due primarily to elimination of suspect data sets having poor documentation, apparent inconsistencies and/or highly atypical results. It was not possible to rationally eliminate other data sets based on the information available.

2.3. Statistical Analysis of data scattering

In view of an inability to obtain data needed to determining which data sets were most reliable, it was decided to use a purely

statistical approach to select sets of data that might be assumed most “reliable”. To do this, the mean value and standard deviation of sway force and yaw moment were determined using all data sets of Figures 2.1 and 2.2, for each of the 29 non-trivial combinations of drift angle and yaw rate. These values were used to determine, for sway force and yaw moment for each of the N data sets and each combination of drift angle and yaw rate, a difference of the value from the mean value for all data sets. The “deviation” of a data set was then defined to be the average, for all combinations of drift angle and yaw rate, of the difference of the values from the mean value, divided by the standard deviation, or:

$$D_n = \{ \sum_m [(F_n(\beta_m, r'_m) - F_{\text{mean}}(\beta_m, r'_m)) / \sigma(\beta_m, r'_m)] \} / M$$

where:

D_n is average deviation of sway force or yaw moment, F , for test data set n ;

$F_n(\beta_m, r'_m)$ is force or moment for n -th data set and m -th set of values of β and r' ;

$F_{\text{mean}}(\beta_m, r'_m)$ is mean value of force for all data sets for m -th set of values of β and r' ;

$\sigma(\beta_m, r'_m)$ is standard deviation for all data sets for m -th set of values of β and r' ;

M is the total combinations of β and r' , considered, $M = 29$, $m = 1, \dots, 29$

N is total number of data sets considered, $n = 1, \dots, N$.

Values of the “deviation”, D_n , for each data sets were independently calculated both sway force and yaw moment. Data sets with average “deviations” of about 1.0 or greater were eliminated, and this process was repeated with the resulting reduced data set. Again, data sets with an average “deviation” of about one or more were eliminated, leaving only five remaining data sets for both sway force and yaw moment.

There is no certainty that this statistical process has identified the most reliable data. However, it is encouraging to note that the same data sets were independently selected

for sway force and yaw moment, that the variations of forces and moments among these data sets are quite small.

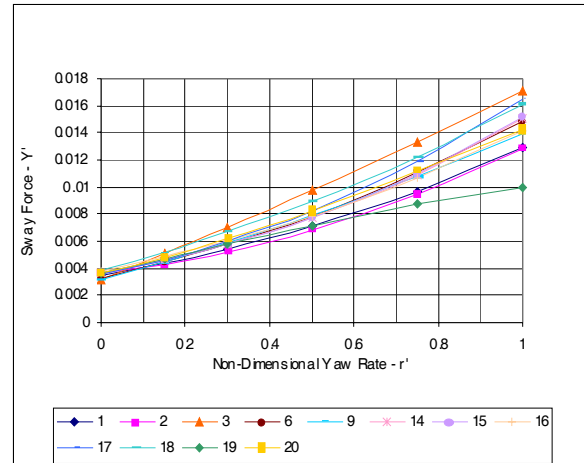


Figure 2.1 Sway forces for $+8^\circ$ drift for selected data set.

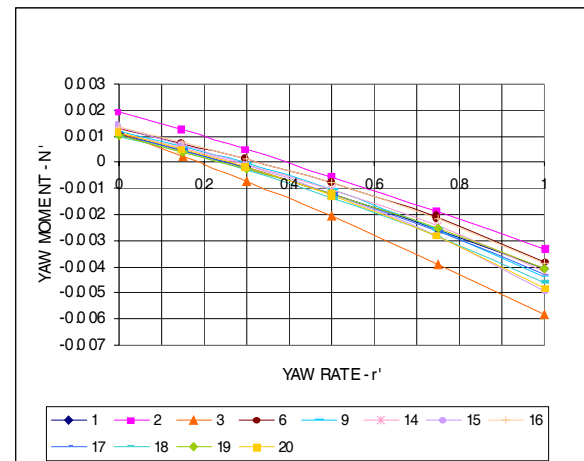


Figure 2.2 Yaw moments for $+8^\circ$ drift for selected data sets.

3. DISCUSSION ON THE REASONS OF SCATTERING

3.1. Potential sources of error with tests

PMM Tests

- The varying rate of rotation during yawing tests
- Inadequate numbers of motion cycles to

eliminate all effects of the starting transient and to permit accurate analysis of the harmonic test data

- Tests at reduced frequencies large enough to introduce unsteady effects in damping forces

Rotating arm test

- Operation of model in its own wake after one revolution
- Requirement to predict acceleration dependant forces which cannot be measured.

Systems identification (SI) of free-running model tests or ship trials data

Systems Identification results are highly sensitive to the quality of the data used and the adequacy of the mathematical model. The sensitivity of the process is illustrated by the differences in the four sets of coefficients obtained using different models by Abkowitz (1984). The validity of SI methods and results has not in the past generally been established by using the identified coefficients to predict maneuvers different than those used for identification.

Model size

- Model forces which are valid only for the conditions (Reynolds number and ambient turbulence level) of the particular test due to laminar flow (scale effects).
- Wall effects when model length is large compared with tank width or diameter, particularly for large PMM motion amplitudes or large static drift angles.

It was concluded by the 22nd ITTC Maneuvering Committee that there was not conclusive evidence of significant scale effects in the available *Esso Osaka* force data, although large differences in forces were observed in coefficients (forces) obtained at BMT using the facilities and the same test procedures for

tests of 1.65 meter and 3.54 meter long models (Dand & Hood, 1983).

3.2. Potential sources of error of data analysis methods

Methods used by various laboratories to analyze captive model test data are rarely described in any detail. These methods can be carried out using:

- Purely mathematical methods, such as regression analysis, using all test data or a data set in which only clearly unreliable data points are eliminated.
- An empirical approach in which the data analyst assigns greater or lesser weight to individual data points based on their experience and knowledge of test conditions.

Data are analyzed or interpreted using a particular mathematical model for hydrodynamic forces. Significantly different individual coefficients can thus be obtained when using the same raw data. Ideally, these coefficients sets will predict similar forces and moments, at least for drift angles, yaw rates, rudder angles and propeller loadings which are most typical of ship maneuvering, although this is by no means certain.

In following parts, the relation among the experimental conditions and analyzing procedures and estimated hydrodynamic forces and the coefficients are discussed.

3.3. Experimental conditions

The measured hydrodynamic forces are changed due to following experimental conditions shown by Yoshimura (2001).

- (1) The center of measuring forces
- (2) The center of captive motion
- (3) The freedom at captive model test

- (4) Error of towing speed
- (5) Experimental condition w/wo propeller
- (6) Propeller loading condition

The center of measuring forces

The measured hydrodynamic forces depend on the position of measuring instrument. Longitudinal force and lateral force are not affected by measuring position. However, measured yaw moment is changed by the position of measuring instrument in the model ship. Generally, motion equations are described based on the center of gravity. However, measuring forces are carried out based on mid-ship position, because the center of gravity of model ship is changed due to loading condition. Therefore, motion's equation are often described based on the center of gravity, using hydrodynamic forces measured at mid-ship position as following. The measured hydrodynamic forces depend on the position of measuring instrument. Longitudinal force and lateral force are not affected by measuring position. However, measured yaw moment is changed by the position of measuring instrument in the model ship. Generally, motion equations are described based on the center of gravity. However, measuring forces are carried out based on mid-ship position, because the center of gravity of model ship is changed due to loading condition. Therefore, motion's equation often described based on the center of gravity using hydrodynamic forces measured at mid-ship position as following,

$$\begin{aligned}
 m\dot{u}_G - mv_G r &= X_G = X \\
 m\dot{v}_G - mu_G r &= Y_G = Y \\
 I_{ZZ}\dot{r} &= N_G = N - x_G Y
 \end{aligned}
 \tag{3.1}$$

where

X, Y, N : hydrodynamic forces measured at mid-ship position

x_G : distance from mid-ship to the center of gravity

The relation between the captive position and the measured hydrodynamic forces

The measuring hydrodynamic forces due to turning motion are affected by the center of turning motion where turning motion is activated. Measured forces are affected by experimental condition. Hydrodynamic coefficients are indicated in different values based on the measuring point of Hydrodynamic forces and center of enforced motion.

Table 3.1 shows the hydrodynamic coefficients based on different expression.

Table 3.1 Hydrodynamic coefficients acting on bare hull *Esso Osaka* (Model ship length 2.5 m).

<i>Motion</i>	CG	CG	Mid ship
<i>Moment</i>	CG	Mid ship	Mid ship
X'_{vv}	0.0218	0.0218	0.0216
$X'_{vr}-m_y$	0.1871	0.1871	0.1905
X'_{rr}	0.0062	0.0062	0.0122
X'_{vvv}	0.2786	0.2786	0.2743
Y'_v	-0.3901	-0.3789	-0.3786
$Y'_{r}-m_x$	0.0702	0.0556	0.0435
Y'_{vvv}	-1.2407	-1.2208	-1.2231
Y'_{vvr}	0.2927	0.2644	0.1485
Y'_{vrr}	-0.3387	-0.3190	-0.3070
Y'_{rrr}	0.0594	0.0536	0.0441
N'_v	-0.1263	-0.1437	-0.1439
N'_r	-0.0622	-0.0533	-0.0577
N'_{vvv}	-0.0597	0.0115	0.0120
N'_{vvr}	-0.2341	-0.2118	-0.2164
N'_{vrr}	0.0994	-0.0795	0.0657
N'_{rrr}	-0.0149	-0.0103	-0.0081

The methods of installing model

To measure the hydrodynamic forces on surge, sway and yaw, the motions on these directions are fixed. The fixing condition of other 3 motions such as pitch, roll and heave

affect the measuring hydrodynamic forces in following cases.

In case of small GM at model test, the big heeling angle induces the measuring hydrodynamic forces corresponding to that condition. GM at model test must be same as full-scale ship. In case of cramping the pitching and heaving motion, the measuring hydrodynamic forces are measured under the condition without sinkage. They differ from free running condition in which sinkage is occurred depending on ship speed.

The experimental condition

When the hydrodynamic forces acting on hull are estimated, the experimental condition gives several effects on them. It is proper way to carry out the captive model test using bare hull. However, to reduce the experiment numbers, the captive test are carried out with propeller and rudder. And the hydrodynamic forces acting on hull are estimated by subtracting propeller and rudder forces and their interaction forces from measured total forces. The estimated hydrodynamic forces acting on hull by this way often show difference from forces by measuring bare hull. As, the flow at stern is affected by propeller and rudder, they show difference ones. Especially, the suction force caused by propeller affect the estimated forces acting on hull.

The effect of propeller loading condition on forces acting on hull

The hydrodynamic forces acting on hull are affected by propeller's loading condition. Table 3.2 shows the relation between the hydrodynamic forces acting on hull and propeller loading conditions. The hydrodynamic forces acting on hull measured in the condition of bare hull and in condition of propeller and rudder equipped are shown. The propeller loading are ship point and model point.

Table 3.2 Estimated Hydrodynamic coefficients *Esso Osaka* (Model ship length 2.5 m).

	without Propeller	Ship point	Model point
X'_{vv}	0.0216	0.0401	0.0150
X'_{vr-m_y}	0.1905	0.1830	0.1946
X'_{rr}	0.0122	0.0138	0.0116
X'_{vvv}	0.2743	0.1419	0.3172
Y'_v	-0.3786	-0.3718	-0.3838
Y'_{r-m_x}	0.0435	0.0572	0.0613
Y'_{vvv}	-1.2231	-1.3804	-1.2312
Y'_{vvr}	0.1485	-0.0341	0.0128
Y'_{vrr}	-0.3070	-0.2713	-0.2882
Y'_{rrr}	0.0441	0.0014	0.0092
N'_v	-0.1439	-0.1432	-0.1456
N'_r	-0.0577	-0.0560	-0.0578
N'_{vvv}	0.0120	-0.0004	0.0049
N'_{vvr}	-0.2164	-0.2534	-0.2407
N'_{vrr}	0.0657	0.0331	0.0341
N'_{rrr}	-0.0081	-0.0138	-0.0115

Error of towing speed

When CMT is carried out, the velocity of each towing carriage is controlled based on calculated velocity. As the motion characteristic of each towing carriage is different, actual motion of each carriage cannot realize the calculated motion. Error of towing speed makes the affect on the measuring hydrodynamic force.

Figure 3.1 shows one example of the relation between the turn rate and combined speed of towing carriage.

Table 3.3 shows corrected hydrodynamic forces based on the characteristics of towing carriage motions and measured ones. The hydrodynamic coefficients concerning turn rate (r) are changed.

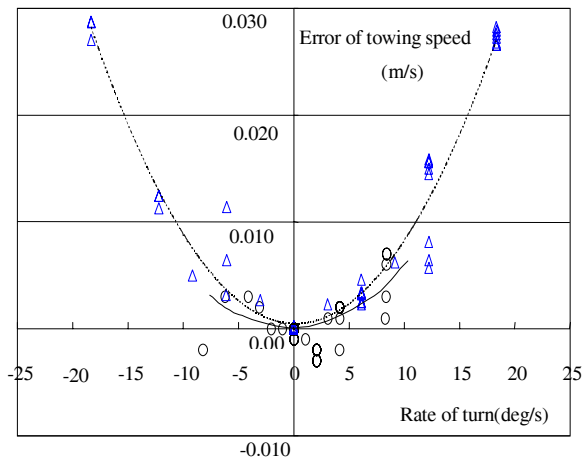


Figure 3.1 The characteristics of towing carriage in CMT.

Table 3.3 Hydrodynamic coefficients measured by CMT (Model ship length 2.5 m).

Motion: Midship Moment: Midship	Corrected Hydrodynamic Forces	Measured Hydrodynamic Forces
X'_{vv}	0.0216	0.0378
$X'_{vr}-m_v$	0.1905	0.1834
X'_{rr}	0.0122	0.0178
X'_{vvv}	0.2743	0.1753
Y'_v	-0.3786	-0.3793
Y'_r-m_x	0.0435	0.0331
Y'_{vv}	-1.2231	-1.2419
Y'_{vvr}	0.1485	0.0162
Y'_{vrr}	-0.3070	-0.2521
Y'_{rrr}	0.0441	0.0563
N'_v	-0.1439	-0.1438
N'_r	-0.0577	-0.0613
N'_{vv}	0.0120	0.0095
N'_{vvr}	-0.2164	-0.2217
N'_{vrr}	0.0657	0.0555
N'_{rrr}	-0.0081	-0.0045

3.4. Conclusions

It has not been possible to explain the very large differences in forces calculated using hydrodynamic coefficients reported by the 22nd ITTC Maneuvering Committee. There are many possible sources of differences, but no primary sources have been clearly identified. 15 to 20 years after most tests *Esso Osaka* tests were carried out, raw data are largely unavailable and many of those responsible for tests and data analysis are no longer active. It is therefore concluded that the reasons for the large observed data scatter must remain largely undefined.

4. DISCUSSION ON THE TRIAL AND FREE RUNNING MODEL TEST

4.1. Full scale trial

The potential inaccuracies of any ship trials data are well recognized. These inaccuracies arise from the difficulty in correcting measured results for effects of temporally and spatially varying wind, current and waves and inaccuracies in basic measurements such as ship position. The special maneuvering *Esso Osaka* trials of 1979 were planned and carried out with unusual care, but available sensors technology at that time was relatively unsophisticated, particularly the pre-GPS equipment used to record ship track. Finally, deep water trials were carried out at a mean water depth-to-draft ratio of 4.2, where bottom effects could exist, and water depth was not constant in the shallow water trials despite the great effort taken to select trials locations where water depth was nearly constant.

Table 4.1 shows the main contents of sea trial in deep water conditions. Figure 4.1 shows the turning trajectory with right rudder angle 35 degrees and Figure 4.2 shows the results of 10/10 zigzag maneuver.

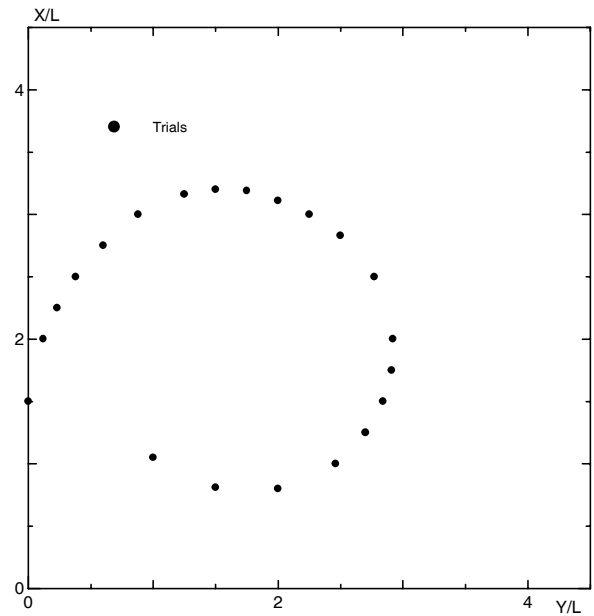
4.2. Free running model tests

The measured turning motion of free running models was used in evaluating the accuracy of simulations. Three sets of free running model turning motion test results were available to be used. Two sets of tests were carried out using models of 2.5 m in length and one was carried out using a model of 4.6 m in length.

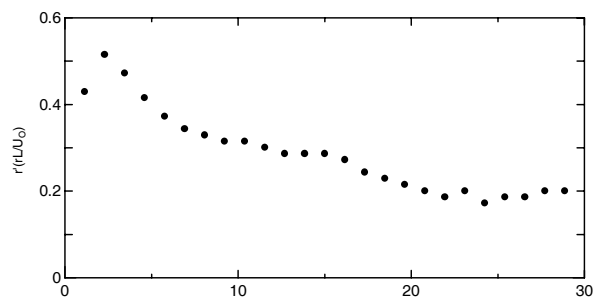
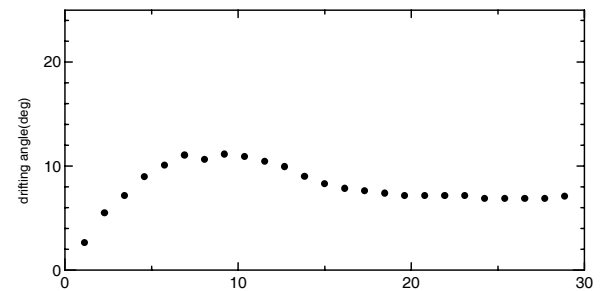
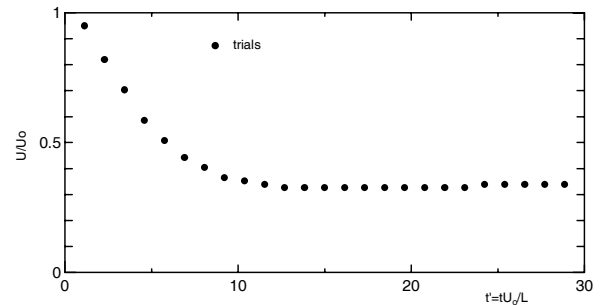
Table 4.1 Main contents of Sea Trial (deep water condition).

Type of Trial	Rudder angle or Rudder/heading angle (deg)	Speed of Approach (knots)
Turning maneuver	35, left rudder	7
Turning maneuver	35, right rudder	7,10
Coasting turning maneuver	35, left rudder	5
Zigzag maneuver	20/20	7
Coasting Zigzag maneuver	20/20	5
Zigzag maneuver	10/10	7

Mean trajectories for these 3 models are shown in Figure 4.3. A mean trajectory was defined by calculating the mean X position at every unit position on Y axis or by calculating mean Y position at every unit position on X axis. The results for the initial stage of turning show significant differences, although steady turning radii are nearly identical, ranging from $2.45L$ to $2.48L$. The reasons for the difference in initial turning shown in Figure 4.3 are not clear. Therefore, the mean trajectory of the 3 tests was used as a baseline turning motion for free running model tests.



a. The turning trajectory in Trial



b. The time history on ship's speed, drifting angle and rate of turn

Figure 4.1 The result of turning maneuver in trial.

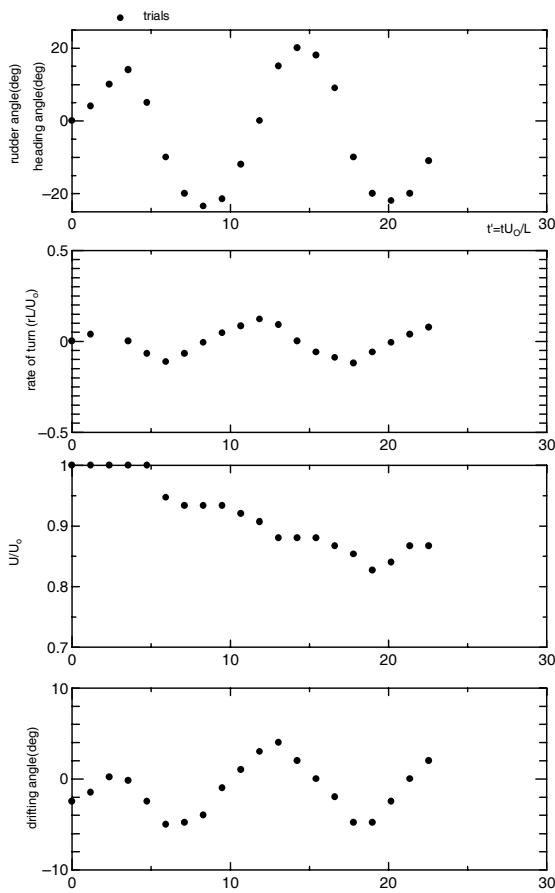


Figure 4.2 Zigzag maneuver in Trial (10/10 Zigzag).

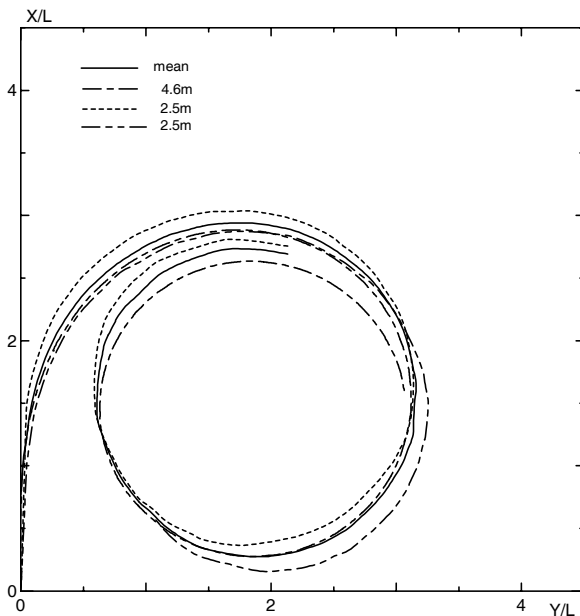


Figure 4.3 The turning trajectory in free running model test (rudder angle $+35^\circ$).

5. SIMULATION STUDIES ON MMG MODEL

5.1. Mathematical model on MMG

Basic equation of motion

The mathematical model used in this study is shown below.

$$\left. \begin{aligned} m\dot{u} - mvr &= X \\ m\dot{v} + mur &= Y \\ I_{zz}\dot{r} &= N - x_G Y \end{aligned} \right\} \quad (5.1)$$

where:

the origin of maneuvering motion is at the center of gravity of the ship;

the origin of hydrodynamic force is at the midship section on the centerline of the ship.

m : mass of a ship, I_{zz} : moment of inertia of yawing, X , Y and N are hydrodynamic forces and moment acting on midship. x_G represents the location of C.G. in x -axis direction from the midship.

These hydrodynamic forces and moments can be divided into the following components.

$$\left. \begin{aligned} X &= X_H + X_P + X_R \\ Y &= Y_H + Y_P + Y_R \\ N &= N_H + N_P + N_R \end{aligned} \right\} \quad (5.2)$$

where subscripts H , P and R refer to hull, propeller and rudder, respectively. Interaction between hull and propeller and among hull, propeller and rudder are contained in forces and/or moment with subscript P and R .

Hydrodynamic forces and moment acting on the hull

Hydrodynamic forces and yaw moments acting on the hull are as follows:

$$\left. \begin{aligned} X'_H &= -m'_x \dot{u}' X'(0) + X'_{vv} v'^2 + (X'_{vr} - m'_y) v' r' \\ &\quad + X'_{rr} r'^2 + X'_{vvv} v'^4 \\ Y'_H &= -m'_y \dot{v}' + Y'_{vv} v' + (Y'_{vr} - m'_x) r' + Y'_{vvv} v'^3 \\ &\quad + Y'_{vvr} v'^2 r' + Y'_{vrr} v' r'^2 + Y'_{rrr} r'^3 \\ N'_H &= -J'_{zz} \dot{r}' + N'_{vv} v' + N'_{vr} r' + N'_{vvv} v'^3 \\ &\quad + N'_{vvr} v'^2 r' + N'_{vrr} v' r'^2 + N'_{rrr} r'^3 \end{aligned} \right\} (5.3)$$

$$X_R = -(1 - t_R) F_N \sin \delta \quad (5.10a)$$

$$Y_R = -(1 + a_H) F_N \cos \delta \quad (5.10b)$$

$$N_R = -(x_R + a_H x_H) F_N \cos \delta \quad (5.10c)$$

5.2. Hydrodynamic forces acting on hull

$X(0)$ are measured from resistance test.

Hydrodynamic forces induced by propeller

The hydrodynamic forces induced by the propeller are expressed as below:

$$X_P = (1 - t) T = \rho D_P^4 n^2 (1 - t) K_T \quad (5.4)$$

$$K_T = a_1 + a_2 J + a_3 J^2 \quad (5.5)$$

$$J = \frac{u_P}{n D_P} \quad (5.6)$$

$$u_P = u(1 - w_P) \quad (5.7)$$

where t : thrust deduction factor, n : propeller revolution, D_P : propeller diameter, J : propeller advance ratio, a_1 , a_2 and a_3 : constant for propeller open characteristics

On wake fraction $1 - w_P$, various estimation formulas are proposed. Following two mathematical models were used in this study.

[model 1]

$$1 - w_P = 1 - w_{P0}(J_P) + k_{w1}(\beta - l_P r') + k_{w2}(\beta - l_P r')^2 \quad (5.8a)$$

$$1 - w_{P0}(J_P) = a_{w0} + a_{w1} J_P + a_{w2} J_P^2 \quad (5.9)$$

[model 2]

$$1 - w_P = (1 - w_{P0}) + \tau |v' + x'_P r'| + C'_P (v' + x'_P r')^2 \quad (5.8b)$$

Hydrodynamic force and yaw moment induced by rudder

The hydrodynamic forces induced by rudder are described below, in terms of rudder normal force F_N , rudder angle δ , and rudder to hull interaction coefficients t_R , a_H , x_H :

As stated previously, hydrodynamic coefficients can have different values as a result of differences of experimental condition, analysis procedures and mathematical models used. The effect of these issues on the data being considered here cannot be quantified. Therefore, it is not meaningful to compare the different sets of data directly.

Data from four sets of tests for which detailed information were available for consideration. The hydrodynamic coefficients obtained from these four sets of tests using different procedures, were unified to a single set of test conditions and the unified data were used to simulate maneuvering of the *Esso Osaka*.

The experimental conditions for the four selected tests are shown in Table 5.1. Bare hull hydrodynamic coefficients derived from the test results, unified to the same test conditions, are shown in Table 5.2. Longitudinal hydrodynamic forces for the 4 model ships are shown in Figure 5.1. Lateral force and yawing moment are shown in Figure 5.2 and Figure 5.3. In Table 5.2 and in all figures showing hydrodynamic forces, mean hydrodynamic coefficients, and resulting mean hydrodynamic forces, calculated using each of the 4 models, are also shown.

Longitudinal forces, X' , for the 4 model shown in Figure 5.1 show similar tendency for small drift angles and turning rates. With large yaw rate and drift angle or sway rate, the hydrodynamic forces show significant differences. Lateral force, Y' , shows a similar tendency but with smaller difference than those for X' . Yaw moment, N' , also shows similar tendency, with the differences between the 4 sets of hydrodynamic forces increase as the combined yaw and sway rates increase.

Table 5.1 Experimental conditions.

Research Institute	A	B	C	D
Length of model ship	6.0 m	4.6 m	4.0 m	2.5 m
Kind of test	C.M.T.	C.M.T.	C.M.T.	C.M.T.
Model ship speed Froude Number	0.699 m/s, $Fn=0.0912$	0.611 m/s, $Fn=0.0910$	0.400 m/s, $Fn=0.0639$	0.450 m/s, $Fn=0.0911$
Revolution of propeller	ship point	model point	bare hull	model point
appendages	Propeller, rudder	Propeller, rudder	none	Propeller, rudder
Measured items	Hull forces, propeller thrust, rudder normal forces	Hull forces, propeller thrust, rudder normal forces	Hull forces	Hull forces, propeller thrust, rudder normal forces
Captive point	C.G.	C.G.	C.G.	C.G.
The measurement center of the yaw moment	Mid Ship	C.G.	C.G.	Mid Ship
Freedom of ship motion	Fore: pitching Free Aft.: pitching & surging Free	Free to pitching, rolling	Free to pitching, heave, rolling	Free to pitching, rolling
Experimental range	O.T: $\beta=\pm 0\div 30^\circ$ CMT: $r'=\pm 0\div 1.0$ Coupling motion range at CMT ($r'=0\div 0.8, \beta=-20\div 20.0^\circ$) ($r'=0\div -0.8, \beta=-20\div 20.0^\circ$)	O.T: $\beta=\pm 0\div 30^\circ$ CMT: $r'=\pm 0\div 0.5$ Coupling motion range at CMT ($r'=0\div 0.8, \beta=0\div 30^\circ$) ($r'=0\div -0.8, \beta=0\div -30^\circ$)	O.T: $\beta=\pm 0\div 20^\circ$ CMT: $r'=\pm 0\div 0.8$ Coupling motion range at CMT ($r'=0\div 0.8, \beta=0\div 20.0^\circ$) ($r'=0\div -0.8, \beta=0\div 20.0^\circ$)	O.T: $\beta=\pm 0\div 25^\circ$ CMT: $r'=\pm 0\div 0.8$ Coupling motion range at CMT ($r'=0\div 0.8, \beta=-5\div 17.5^\circ$) ($r'=0\div -0.8, \beta=5\div -17.5^\circ$)

While the different methods of captive model test and different analyzing procedures were done, we can compare the unified values by coherent converting way concerning the contents. As a result, it is clarified that the scattering among them are small. In next section, the effects of the varieties in data on the estimation of motion are discussed.

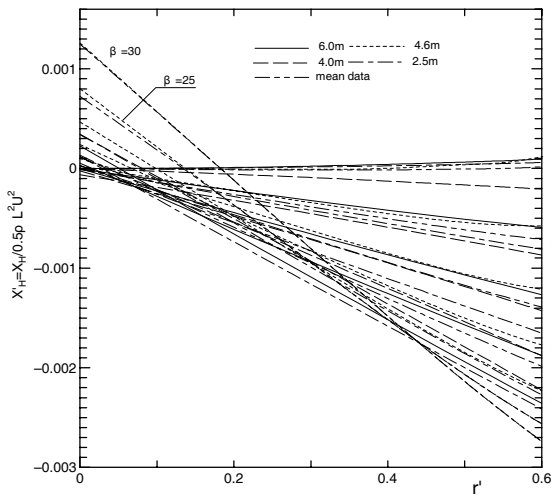


Figure 5.1 Longitudinal force (X'_H).

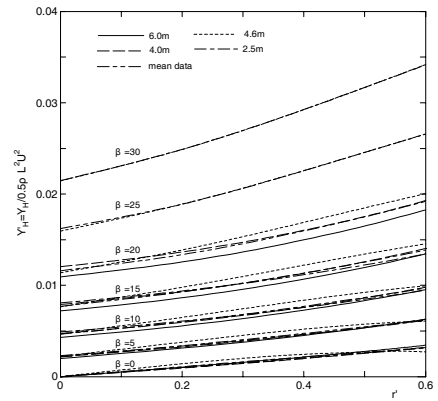


Figure 5.2 Lateral force (Y'_H).

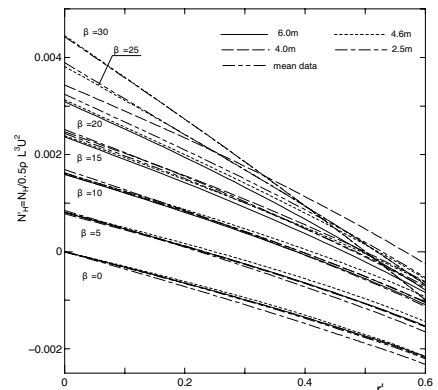


Figure 5.3 Yaw moment (N'_H).

Table 5.2 Hydrodynamic coefficients.

	6.0 m	4.6 m	4.0 m	2.5 m	Mean data
Motion	C.G.	C.G.	C.G.	C.G.	C.G.
Moment	Mid Ship	Mid Ship	Mid Ship	Mid Ship	Mid Ship
Propeller revolution	Ship point	Model point	—	Model point	—
appendages	Propeller & rudder	Propeller & rudder	—	Propeller & rudder	—
X'_{vv}	-0.01046	-0.01046	-0.00344	0.00489	-0.00329
X'_{vvv}	0.33753	0.22216	0.22750	0.33705	0.277875
X'_{rr}	0.00388	0.00337	-0.00962	0.00250	3.4E-05
$X'_{vr}+m_{y'}$	0.19490	0.17073	0.16046	0.24980	0.183616
Y'_v	-0.33231	-0.37003	-0.36152	-0.38348	-0.3831
$Y'_r-m_{x'}$	0.07543	0.11050	0.06934	0.07330	0.082145
Y'_{vv}	-1.23856	-1.08291	-1.40179	-1.22775	-1.05375
Y'_{vvr}	0.16712	0.40898	0.15960	0.13322	0.59837
Y'_{vrr}	-0.37771	-0.48898	-0.39704	-0.29181	-0.25589
Y'_{rrr}	0.02868	-0.11900	0.02742	0.01818	-0.01119
N'_v	-0.13800	-0.13974	-0.13282	-0.14540	-0.14716
N'_r	-0.04779	-0.04485	-0.04758	-0.05323	-0.04836
N'_{vv}	0.02644	0.02736	-0.14675	0.00449	0.053257
N'_{vvr}	-0.29422	-0.33238	-0.26843	-0.23498	-0.29699
N'_{vrr}	0.04047	-0.00461	0.02922	0.04983	0.023637
N'_{rrr}	-0.01673	-0.02493	-0.01903	-0.01268	-0.01835

Non-dimensional forms: $X'_H = X_H / \frac{1}{2} \rho L d U^2$, $Y'_H = Y_H / \frac{1}{2} \rho L d U^2$, $N'_H = N_H / \frac{1}{2} \rho L^2 d U^2$

5.3. Estimation on ship's motion

Estimation using original proposed data

For studying the effect of different hydrodynamic forces acting on hull, the forces caused by propeller and rudder were estimated using the following mathematical model, des-

ignated PR model-1, and the associated coefficients given in Table 5.3.

Table 5.3 The coefficient in (PR model-1).

$1-w_{p0}$	τ	C'_p	x'_p	k	ε
0.386	0.871	-0.359	-0.517	0.288	1.420

(PR model-1)

$$1 - w_D = (1 - w_{D0}) + \tau |v' + x'_D r'| + C'_D (v' + x'_D r')^2 \tag{5.10}$$

$$\frac{u_R}{u_P} = \varepsilon + k(\sqrt{1 + 8K_T / \pi J^2} - 1) \tag{5.11}$$

$$v_R = \gamma(v' + l_R' r') \tag{5.12}$$

$$\alpha_R = (\delta - \delta_0) + \tan^{-1}(v_R / u_R) \tag{5.13}$$

$$F_N = \frac{1}{2} \rho A_R f_\alpha U_R^2 \sin \alpha_R \tag{5.14}$$

$$U_R = \sqrt{u_R^2 + v_R^2} \tag{5.15}$$

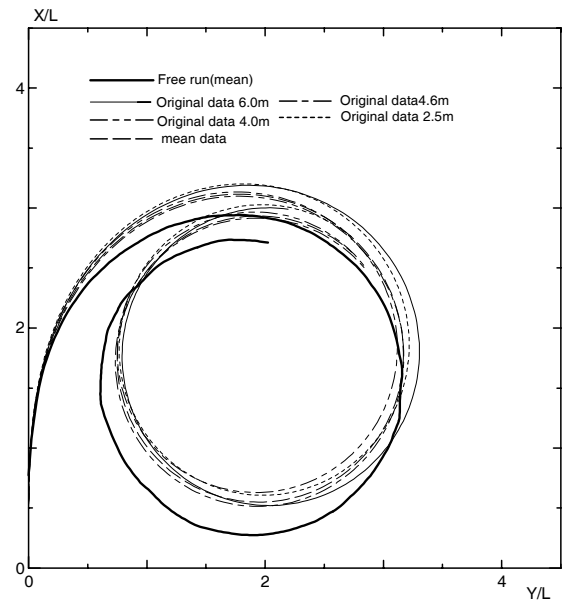
(1) Predicted turning motion

The turning motions estimated using the 4 sets of originally proposed coefficients are shown in Figure 5.4. Turning trajectories are shown in Figure 5.4.a and ship's velocity, drift angle and non-dimensional rate of turn are shown in Figure 5.4.b. Mean results from free-running model tests are also shown in Figures 5.4.a and 5.4.b. All simulated turning trajectories are similar, and the simulated initial turning motions are smaller than the measured initial turning motion. Simulated advances with the different data sets have differences of -0.5% to 2.7% from that simulated using the mean hydrodynamic coefficients, while estimated steady turning diameters have differences of -0.6% to 3.3% from those for the mean hydrodynamic coefficients.

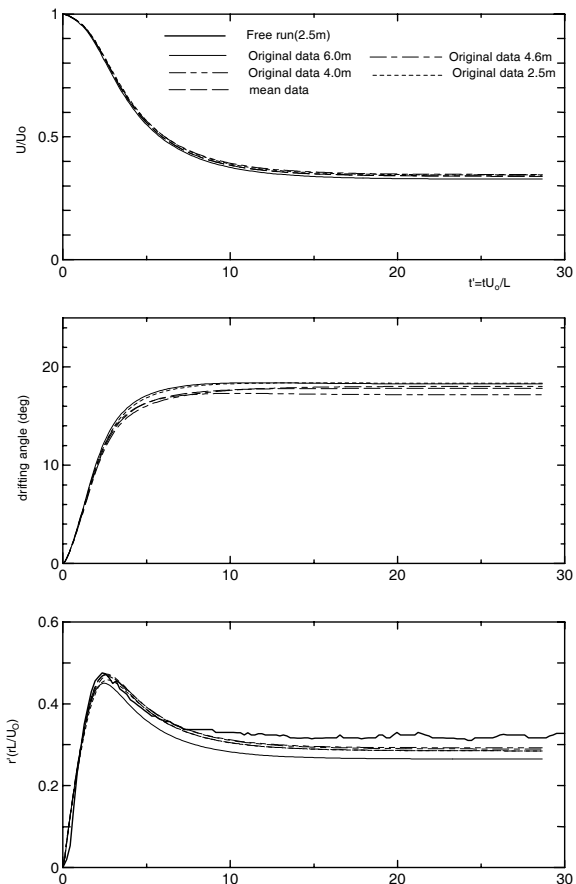
(2) Zigzag test

In Figure 5.5, results for a simulated 15-15 zigzag maneuver results and results for this maneuver obtained from free running tests of a 6.0 m model are presented. The results include rudder angle, turning angle, ship's speed and drift angle. Up to the second overshoot, all simulated results are similar and all are in good agreement with the free running test results.

The difference among the results estimated by using data from each institute shows very small. Concerning the varieties on the results of free running model test, it is difficult to judge whether the data proposed by different institute is good or bad.



a. The turning trajectory (rudder angle +35°)



b. The time history on ship's speed, drifting angle and rate of turn (rudder angle +35°)

Figure 5.4 The estimation of turning motion estimated by using the hydrodynamic coefficients of each institute.

The effect of variety of estimated hydrodynamic forces on motion estimation

It is clarified in previous studies that the effect of difference of estimated hydrodynamic forces shows small. In this section, the effect on simulated motions of changes in an individual hydrodynamic force component, X , Y or N , is discussed.

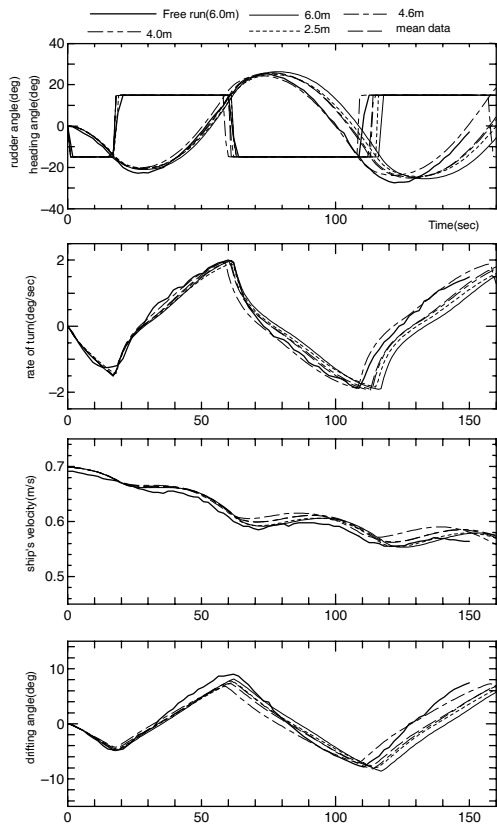
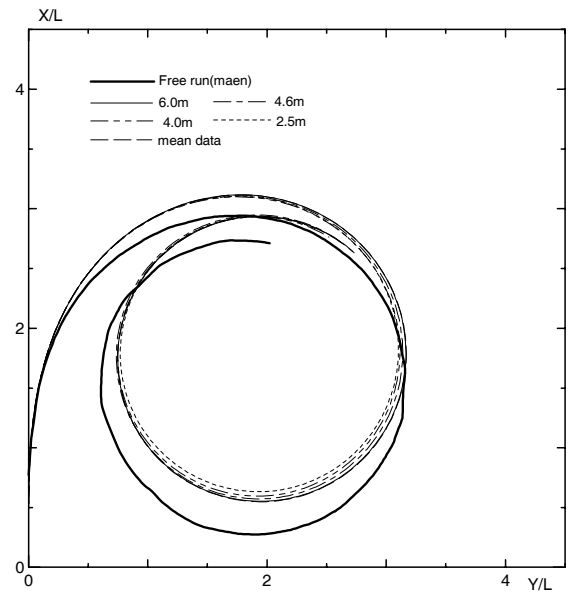


Figure 5.5 The Zigzag maneuver estimated by using the hydrodynamic coefficients of each institute (15/15 Zigzag).

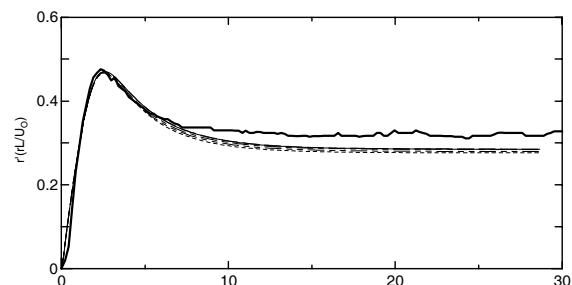
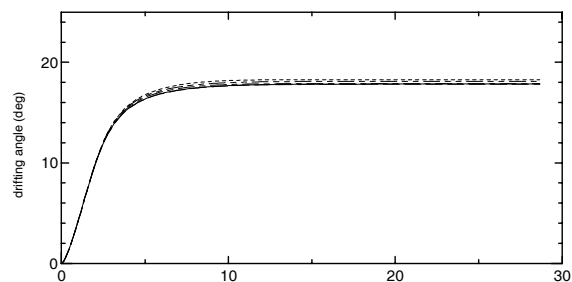
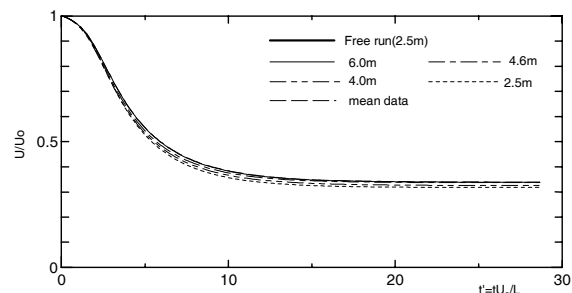
(1) Effect of individual forces on turning motion

(A) The effect of difference in longitudinal force

The effect on simulated results of the difference in the surge force, X , proposed by each institute was studied by conducting simulations in which Y and N were defined to have the mean values for all data. The resulting trajectories are shown in Figure 5.6.a and time histories of ship's speed, drift angle and turn rate are shown in Figure 5.6.b.



a. The turning trajectory (rudder angle $+35^\circ$)



b. The time history on ship's speed, drifting angle and rate of turn (rudder angle $+35^\circ$)

Figure 5.6 The turning motion estimated by using X'_H each institute (Y'_H, N'_H : mean data of each institute are used).

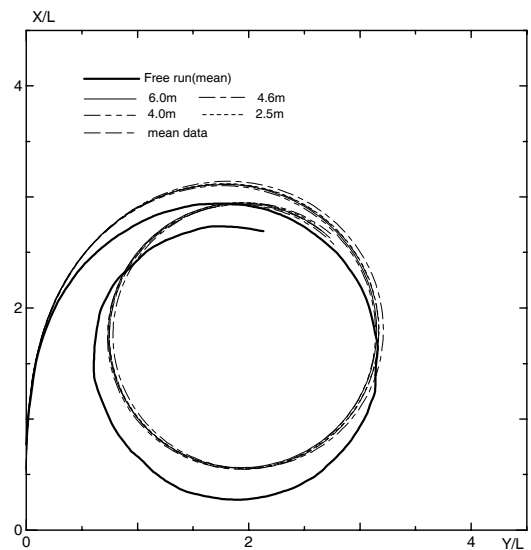
The differences in X , as shown in Figure 5.1, make no significant difference in turning motion. The maximum difference of turning diameter simulated using the four different X forces and the mean hydrodynamic coefficients, the maximum difference of estimated diameter of turning circle is 3.2%, it is very small. For every set of X force data the simulated rate of turn in steady turning motion is smaller than that measured in the free running model tests.

(B) The effect of difference in lateral force

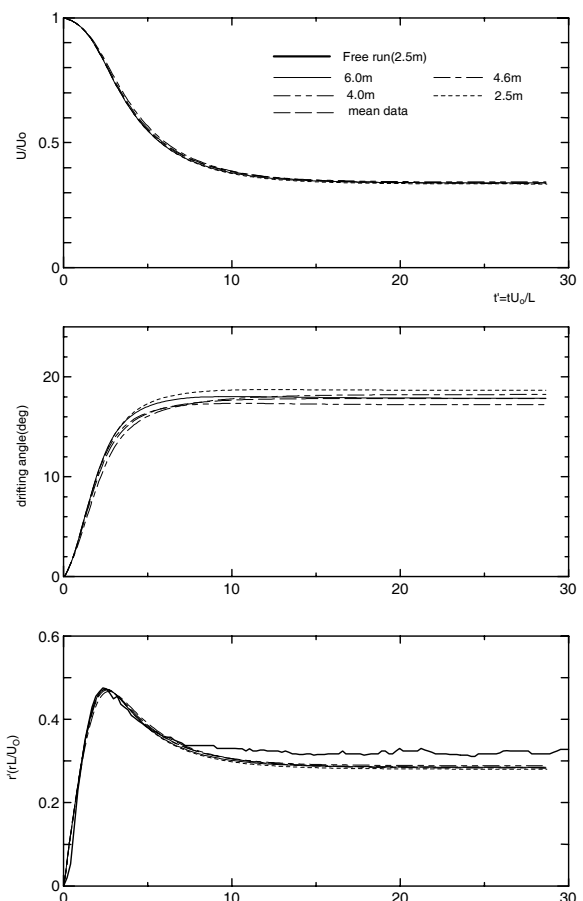
The effect on simulated results of the difference in the surge force, Y , proposed by each institute was studied by conducting simulations in which X and N were defined to have the mean values for all data. The resulting trajectories are shown in Figure 5.7.a, and time histories of ship's speed, drift angle and turn rate are shown in Figure 5.7.b. The differences in Y , as shown in Figure 5.2, make no significant difference in drift angle or in turning motion. The difference of Y_v among the institutes are 13.0% to -0.5% comparing to mean value and the difference of $Y_r - m_x$ are 15.0% to -35.0%. The maximum difference of the advances and turning diameters simulated using the four different Y forces and the mean values of Y are -0.5% to -0.8% and -0.2% to 0.8%, respectively. For every set of Y force data the simulated rate of turn in steady turning motion is smaller than that measured in the free running model tests.

(C) The effect of difference of estimated turning moment

The effect on simulated results of the difference in the yawing moment, N , proposed by each institute was studied by conducting simulations in which X and Y were defined to have the mean values for all data. The resulting trajectories are shown in Figure 5.8.a and time histories of ship's speed, drift angle and turn rate are shown in Figure 5.8.b. Although the differences in N , as shown in Figure 5.3 make no significant difference in turning motion, the turning trajectories show larger differences than do those obtained with different values of X and Y .



a. The turning trajectory (rudder angle $+35^\circ$)



b. The time history on ship's speed, drifting angle and rate of turn (rudder angle $+35^\circ$)

Figure 5.7 The turning motion estimated by using Y'_H each institute (X'_H , N'_H : mean data of each institute).

The difference of N_v among the institutes are 9.5% to 1.0% comparing to mean value and the difference of N_r are 7.0% to -10.%. The maximum difference of the advances and turning diameters simulated using the four different N_s and the mean values are -0.6% to 3.0% and -2.3% to 2.8%, respectively.

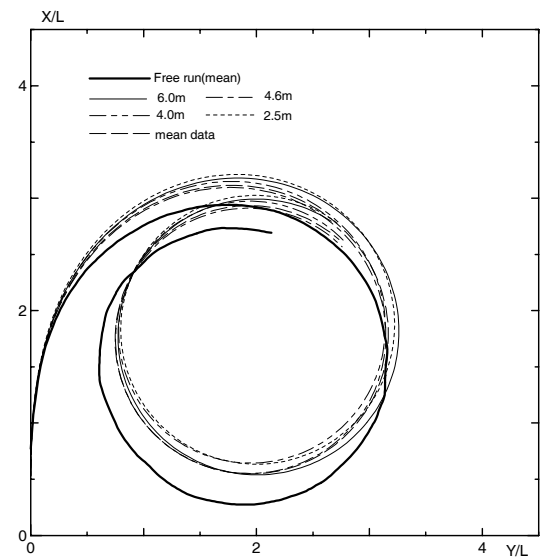
(2) Effect of individual force on zigzag motion

(A) The effect of difference of estimated longitudinal force

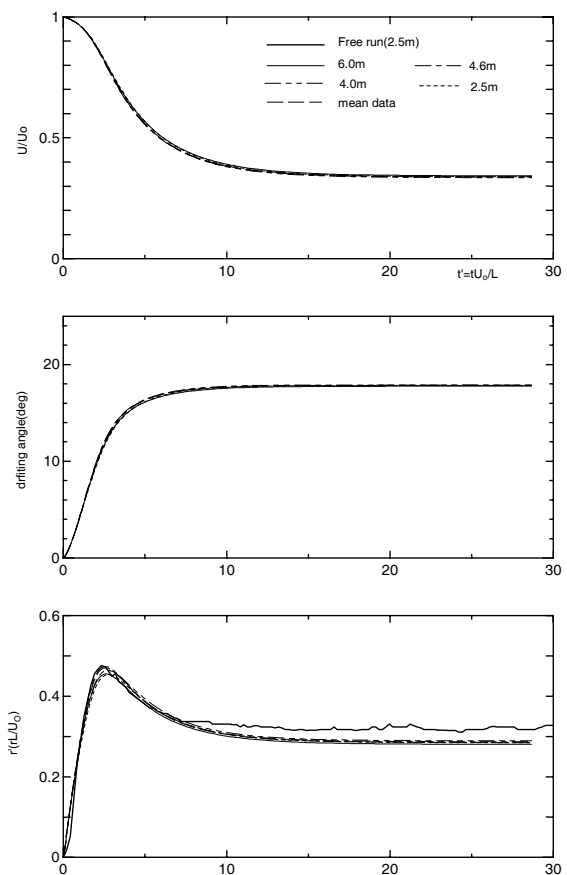
In this section, the effects of difference of longitudinal force X on the zigzag motion estimation are discussed. For this study, the effects of using the X proposed by each institute are discussed, using the mean values of Y and N . Time histories of rudder angle, turning angle, ship's speed and drifting angle are shown in Figure 5.9. The use of the different values of X of Figure 5.1 has no significant effect on zigzag motions, and all results show good agreement with free running model test results up to 2nd overshoot. Comparing to the estimated 1st and 2nd overshoot angles of 5.4 degree and 10.1 degree obtained using mean values of all hydrodynamic coefficients, the different values of X gave values of 5.1 to 5.8 degrees for the 1st overshoot angle and 10.7 to 10.8 degree for the 2nd overshoot angle. These differences are small.

(B) The effect of difference of estimated lateral force

In this section, the effects of difference of lateral force Y on the zigzag motion estimation are discussed. For this study, the effects of Y proposed by each institute are discussed. X and N defined by mean of them are applied. The time histories of rudder angle, turning angle, ship's speed and drifting angle are shown in Figure 5.10. The difference of estimated Y makes big effects on the estimation of overshoot angle and drifting angle. Comparing to the estimated 1st and 2nd overshoot angle by using mean hydrodynamic coefficients that are 5.4 degree and 10.1 degree, the range of estimated 1st overshoot angle is 5.1 to 6.5 degree and the range of estimated 2nd overshoot angle is 9.4 to 12.5 degree.



a. The turning trajectory (rudder angle +35°)



b. The time history on ship's speed, drifting angle and rate of turn (rudder angle +35°)

Figure 5.8 The turning motion estimated by using N'_H each institute (X'_H, Y'_H : mean data of each institute).

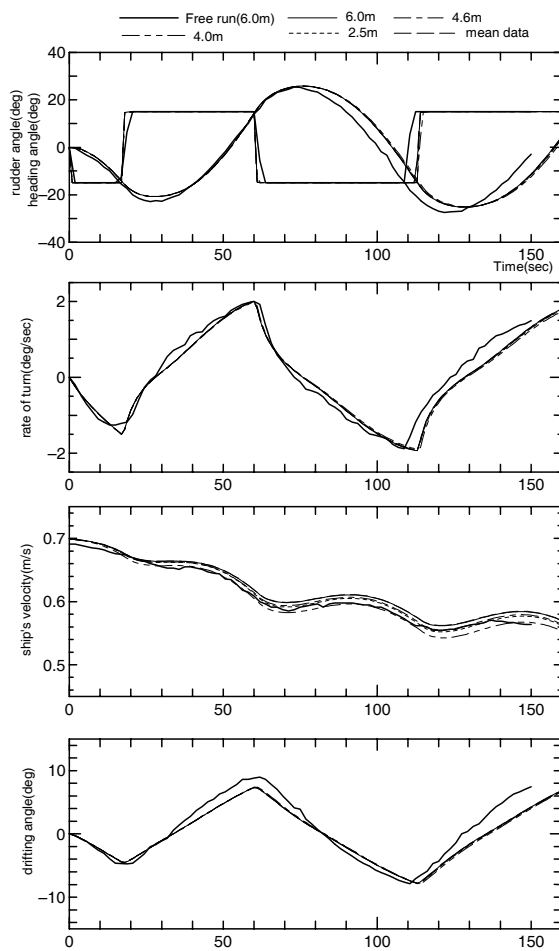


Figure 5.9 The Zigzag maneuver estimated by using X'_H each institute (15/15 Zigzag) (Y'_H , N'_H : mean data of each institute).

(C) The effect of difference of estimated turning moment

In this section, the effects of difference of turning moment N on the motion estimation are discussed. For this study, the effects of N proposed by each institute are discussed. X and Y defined by mean of them are applied. The time histories of rudder angle, turning angle, ship's speed and drifting angle are shown in Figure 5.11. The difference of estimated N shown in Figure 5.3 dose not make big difference on zigzag motion and they show similar estimation up to 2nd overshoot. And they show good agreement to free running model test up to 2nd overshoot angle. Comparing to the estimated 1st and 2nd overshoot angle by using mean hydrodynamic coefficients that are 5.4 degree and 10.1 degree, the range of estimated 1st over-

shoot angle is 5.0 to 5.7 degree and the range of estimated 2nd overshoot angle is 9.3 to 10.5 degree. It is small.

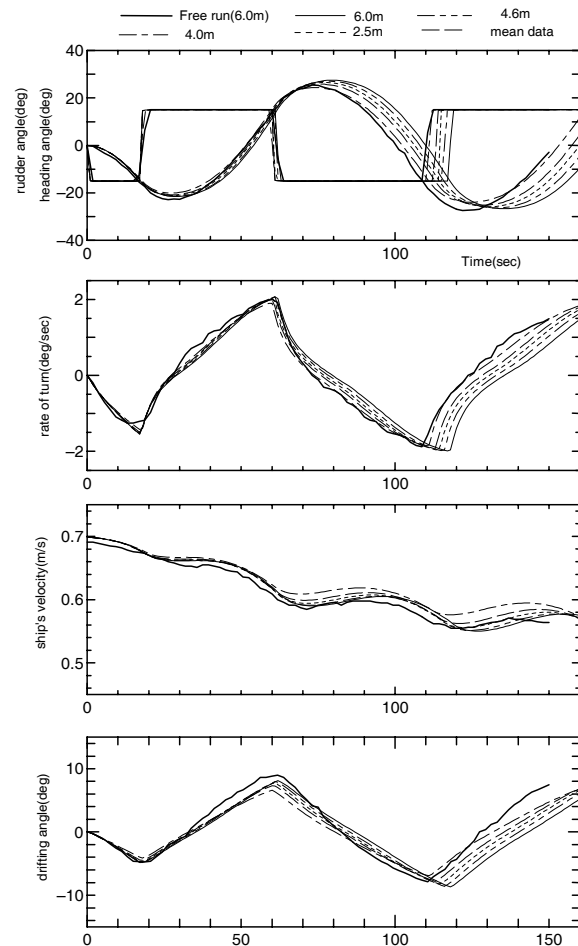


Figure 5.10 The Zigzag maneuver estimated by using Y'_H each institute (15/15 Zigzag) (X'_H , N'_H : mean data of each institute).

As the stability index is defined by certain Y and N coefficients, the change of Y make the change of stability index rather than the change of N . Values of Y_v for the four sets of data differ by 13.0% to -0.5% from the mean value of Y_v and values of $Y_r - m_x$ differ by 15.0% to -35.0% from the mean value. Values of N_v and N_r differ from the mean values by 9.5% to 1.0% and 7.0% to -10.0%, respectively.

The stability index obtained using the original hydrodynamic coefficients proposed by the four institutes differ by 32.0% to -23.0% from those obtained using the mean coeffi-

cients. The range of stability obtained using only individual values of Y differ widely from the mean, by 52.0% to -24.0%. The range of stability indexes due to use of different values only of N is 0% to -26.0%. Therefore, Y forces have a significantly larger effect on stability index than does yaw moments, N . By this reason, the estimated zigzag motions based on the change of Y show bigger scattering rather than ones based on the change of N . Figure 5.12 shows the relation between stability index of bare hull and 1st overshoot angle. The range of stability index due to use of different Y shows wider range than that due to change of N . The accuracy of the Y forces thus has a big effect on the stability index and the accuracy of simulated zigzag motion.

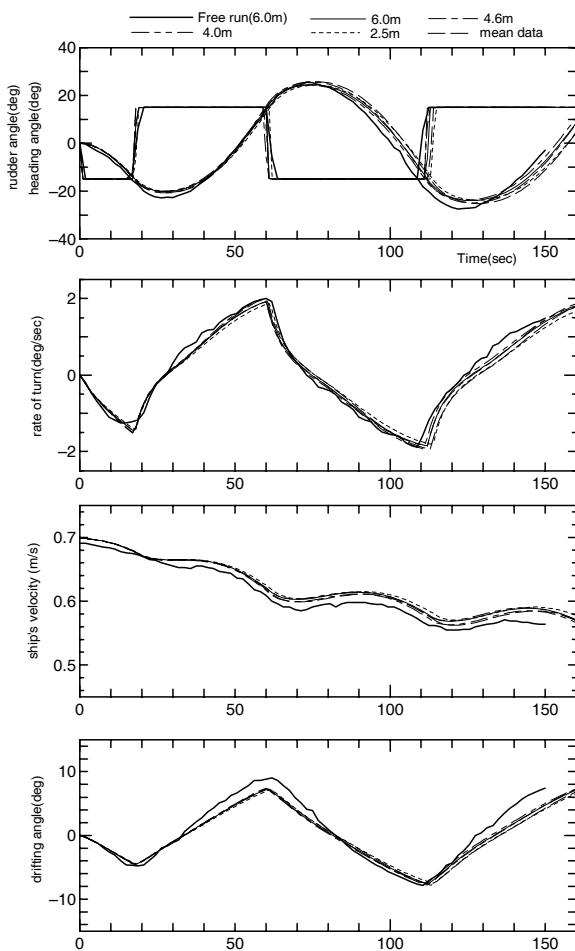


Figure 5.11 The Zigzag maneuver estimated by using N'_H each institute (15/15 Zigzag) (X'_H, Y'_H : mean data of each institute).

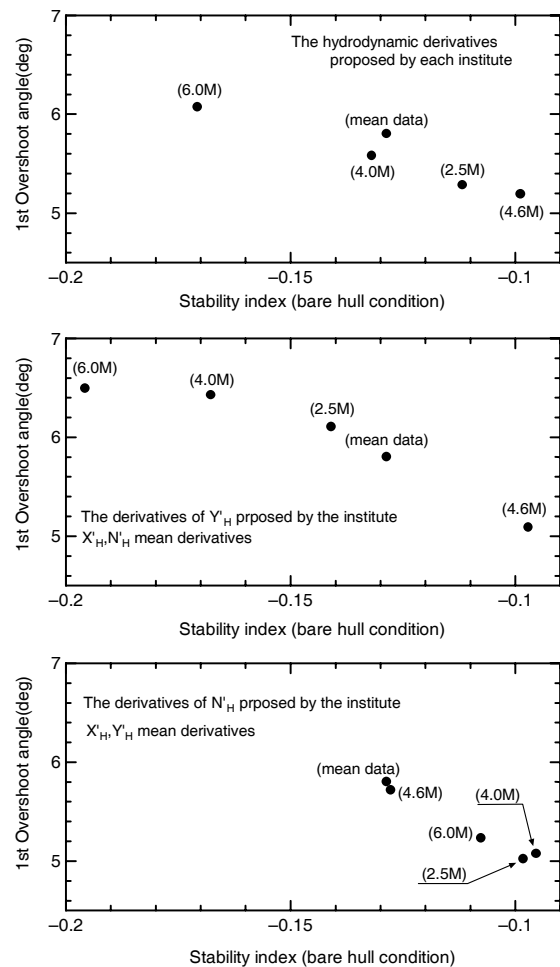


Figure 5.12 The relation between the 1st overshoot angle and stability index.

5.4. Hydrodynamic forces due to propeller, rudder and hull/propeller/rudder interactions

Formulas on Hydrodynamic forces caused by propeller and rudder

Several mathematical models for propeller, rudder and interaction forces have been proposed by different institutes. In this section, the effect on simulated motions of the mathematical model used to predict propeller, rudder and interaction forces is discussed. For this purpose, model PR model-1, which was discussed earlier, and a second model, PR model-2, which is described below, have been used.

(PR model-2)

$$1 - w_P = 1 - w_{P0}(J_P) + k_{w1}(\beta - l'_P r') + k_{w2}(\beta - l'_P r')^2 \tag{5.16}$$

$$1 - w_{P0}(J_P) = a_{w0} + a_{w1}J_P + a_{w2}J_P^2 \tag{5.17}$$

$$\frac{u_R}{u} = (1 - w_R) \sqrt{\eta \left\{ 1 + k \left(\sqrt{1 + \frac{8K_T}{\pi J^2}} - 1 \right) \right\}^2 + (1 - \eta)} \tag{5.18}$$

$$1 - w_R = 1 - w_{R0} + k_{w1}(\beta - l'_P r') + k_{w2}(\beta - l'_P r')^2 \tag{5.19}$$

$$w_{R0} = 1 - \varepsilon(1 - w_{P0}) \tag{5.20}$$

$$-v_R = \delta_R \frac{u_R}{U} \tag{5.21}$$

$$\alpha_R = \delta + \delta_R \tag{5.22}$$

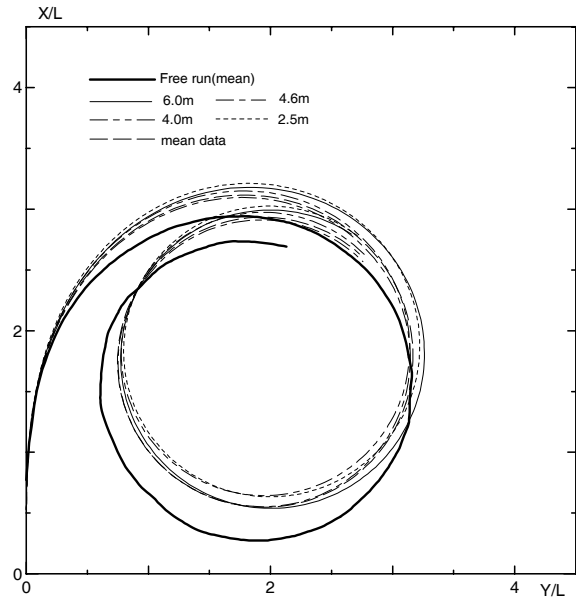
$$F_N = \frac{1}{2} \rho A_R f_\alpha U_R^2 \sin \alpha_R \tag{5.23}$$

$$U_R = \sqrt{u_R^2 + v_R^2} \tag{5.24}$$

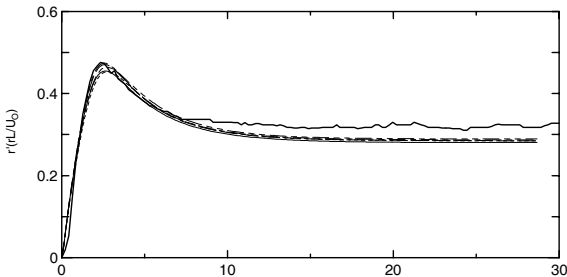
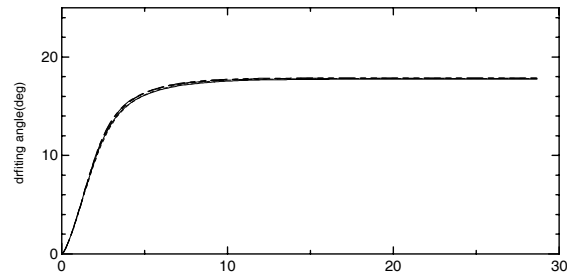
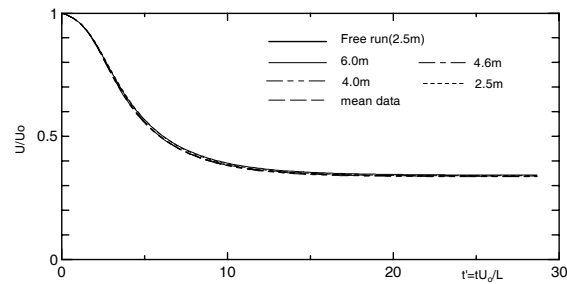
The turning motion simulated using PR model-1 and PR model-2 are shown in Figure 5.13.a. Maximum advance and steady turning diameter estimated using PR model-1 are 3.12L and 2.38L, respectively. Those estimated using PR model-2 are 3.01L and 2.71L. Those measured in free running model test are 2.94L and 2.46L. Figure 5.13.b shows rudder normal force, longitudinal inflow velocity at rudder position and effective inflow angle calculated using both models. The initial stage of turning is estimated different. The differences in the simulated results are due to both the details of the mathematical model and the empirical constants used with each model.

Flow straightening constant

One of specific characteristics of MMG model is to express the hydrodynamic forces caused by propeller and rudder and interaction among hull, propeller and rudder correctly based on the hydrodynamic phenomenon. There are several constant in the PR model-1 mentioned above. The flow straightening constant γ has an important effect on rudder force.



a. The turning trajectory (rudder angle +35°)



b. The time history on rudder normal force, inflow velocity at rudder and effective rudder angle (rudder angle +35°).

Figure 5.13 The turning motion estimated by PR-model-1 and PR-model-2.

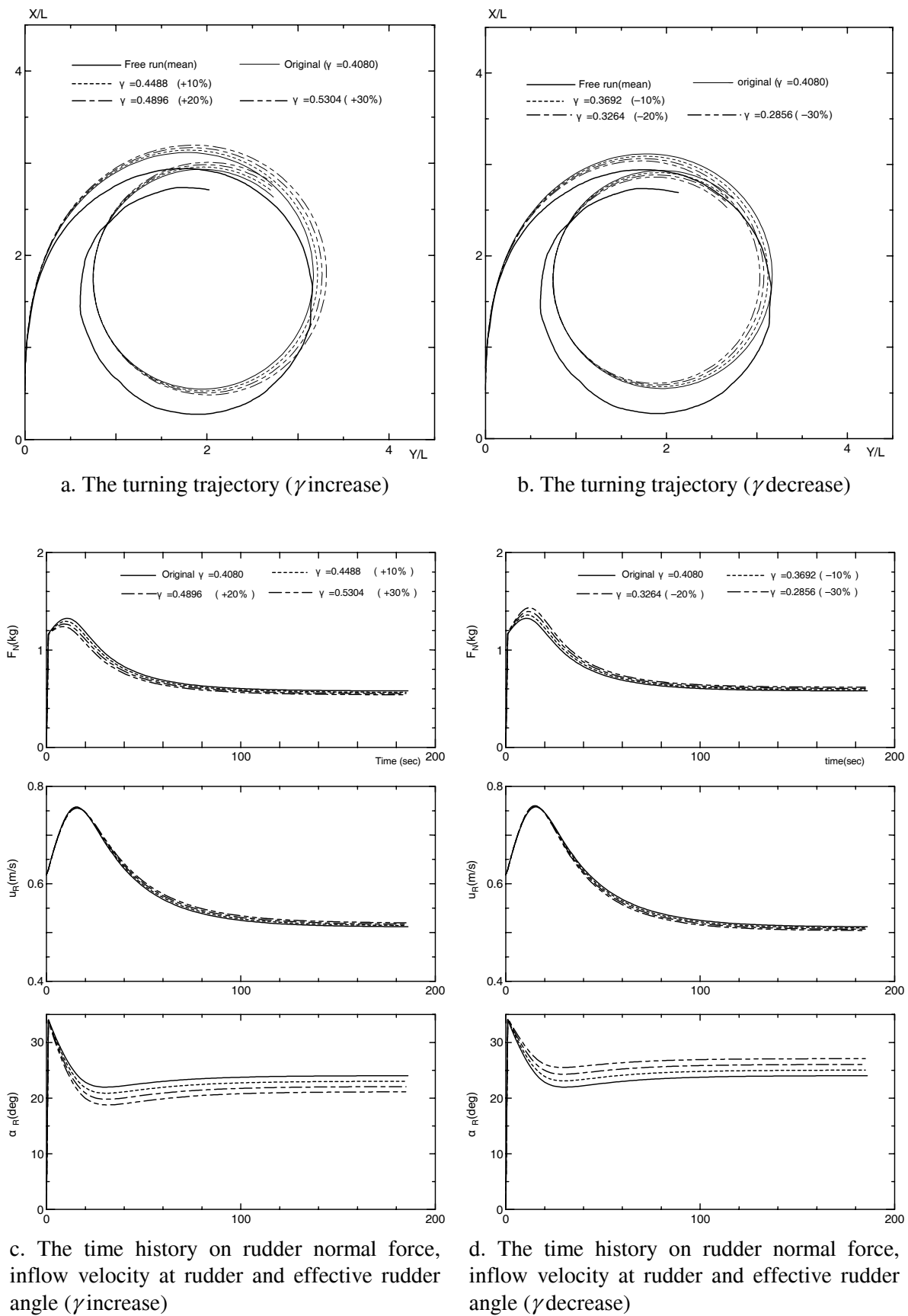


Figure 5.14 The estimation accuracy of γ on turning motion.

Figure 5.14 shows the relation between the turning motion and flow straightening constant. Simulated turning trajectories for incremental increases of 10.0% in the value of γ are shown in Figure 5.14.a and those for 10.0% decreases in the value of γ are shown in Figure 5.14.b. In Figures 5.14.c and 5.14.d, the time histories on rudder normal force, longitudinal flow velocity at the rudder position and effective inflow angle to the rudder are shown. A change in γ results in a change in inflow angle and rudder normal force. The value of γ determines the motion at both the initial stage and steady stage of turning. The effect on turning of the investigated changes of γ is much larger than the effect of the differences in hydrodynamic coefficients.

Constant used with PR model-2

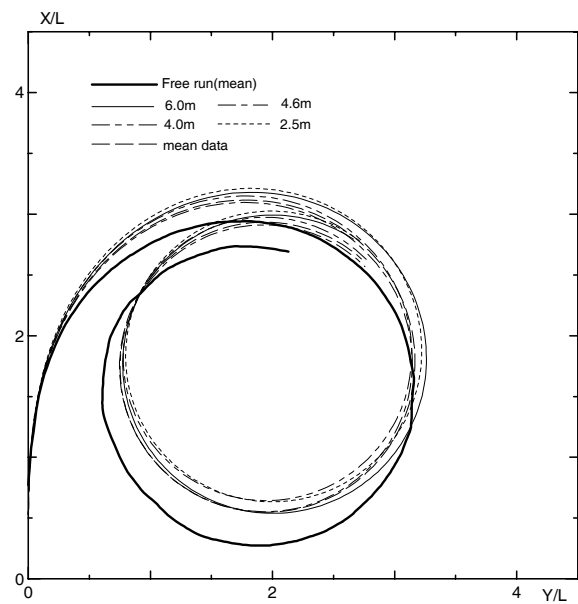
In this section, the effects of element in (PR model-2) are discussed by following methods.

- (1) $(1-w_{P0})$: wake fraction at propeller and propeller loading condition

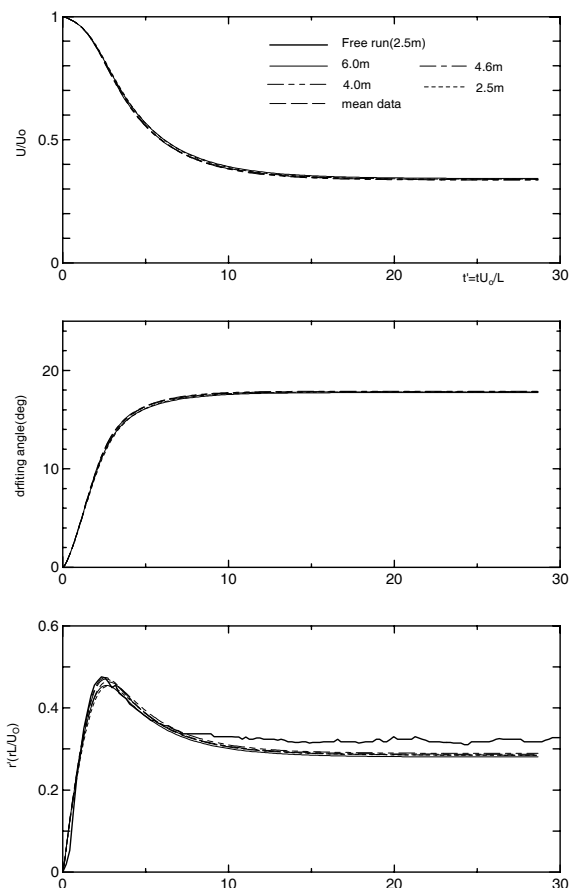
(PR model-2) express that propeller loading condition affects the change of wake fraction at propeller position. We discussed this effect provided that other effects are taken into account. It means that the changes of wake fraction at propeller and rudder position are taken into account.

- (2) $(1-w_P)$: wake fraction at propeller and drifting and yawing condition

(PR model-2) express that drifting and yawing condition affects the change of wake fraction at propeller position. We discussed this effect provided that the following conditions are taken into account. It means that the changes of wake fraction at rudder position are taken into account and wake fraction at propeller position is not affected by propeller loading condition.



a. The turning trajectory (rudder angle $+35^\circ$)



b. The time history on propeller thrust, inflow velocity at rudder and rudder normal force (rudder angle $+35^\circ$).

Figure 5.15 The influence of mathematical model of $1-w_P$ on the turning motion.

Figure 5.15 shows the results of comparison mentioned above. The estimated result containing all of factors in (PR model-2) is also indicated in Figure 5.15. Propeller loading condition in wake fraction at propeller affect small change in motion estimation. On the other hand, when wake fraction at propeller position is assumed as constant during maneuvering motion, propeller advance ratio J is constant. Then the rudder effect is overestimated caused by overestimating longitudinal inflow velocity at rudder position: u_R . Figure 5.15.b shows these situations.

The change of wake fraction due to maneuvering motion has an important effect on propeller and rudder forces and on simulated maneuvering motions.

5.5. Conclusions

The results of available captive model tests reflect differences in experiment condition, mathematical model used, etc. However we can compare hydrodynamic forces proposed by different institutes by unifying them by correcting for differences in test conditions. After such unification, simulated results with the different data show small differences in simulated maneuvering motion. The scattering of results is small because the various institutes understood the concept of the MMG model and thus carried out coherent experiment and analysis of data.

For the future direction, we would like to point out that it is important to carry out experiments and data analysis using a unified approach, and essential to clearly define test conditions and analysis procedures when attempting to compare results from different institutes.

6. SIMULATION STUDIES ON WHOLE SHIP MODEL

As a part of benchmark study, comparative simulations of *Esso Osaka* tanker have been done with selected datasets of ‘whole ship model’ type mathematical model. There are many available datasets of whole ship model type mathematical model which have been submitted to ITTC committee. But it is found that most of them are not suitable for simulation study in this time because of insufficient information on their data and mathematical model. For full simulation, some need further data and some mathematical are not clear. There are also some datasets which are believed to have typographic errors. Therefore, it is not easy to reproduce same simulation results with their original results using only submitted information. For this reason, only three datasets from KRISO (Korea Research Institute of Ships & Ocean Engineering), HSMB (Hydrodynamics Ship Model Basin) and SNU (Seoul National University) are selected as reference datasets.

This section presents the comparison between simulation results by three different models and full-scale trial data. Hydrodynamic forces predicted by three models are also compared each other at the range of motion variables experiencing during standard maneuvers.

6.1. Mathematical models and PMM test results

Mathematical models of ship maneuvering motion, PMM test conditions and hydrodynamic coefficients from three organization are summarized here. All definition of notations and nondimensionalization follows ITTC convention.

KRISO

The mathematical model of KRISO are as follows (Kim, 1988).

$$\begin{aligned}
 m(\dot{u} - vr - x_G r^2) &= X_{\dot{u}} \dot{u} + X_{vr} vr \\
 &+ [X_{vv} + X_{vv\eta}(\eta - 1)]v^2 \\
 &+ [X_{rr} + X_{rr\eta}(\eta - 1)]r^2 \\
 &+ [X_{\delta\delta} + X_{\delta\delta\eta}(\eta - 1)]\delta^2 \\
 &- (\text{Resistance}) + (\text{Thrust})
 \end{aligned} \tag{6.1}$$

$$\begin{aligned}
 m(\dot{v} - ur + x_G \dot{r}) &= Y_o + Y_{o\eta}(\eta - 1) + Y_{\dot{v}} \dot{v} + Y_{\dot{r}} \dot{r} \\
 &+ [Y_v + Y_{v\eta}(\eta - 1)]v \\
 &+ [Y_r + Y_{r\eta}(\eta - 1)]r \\
 &+ [Y_{v|v|} + Y_{v|v|\eta}(\eta - 1)]v|v| \\
 &+ [Y_{r|r|} + Y_{r|r|\eta}(\eta - 1)]r|r| \\
 &+ Y_{vrr}vr^2 + Y_{r|v|}r|v| \\
 &+ [Y_{\delta} + Y_{\delta\eta}(\eta - 1)]\delta \\
 &+ Y_{\delta|\delta|}\delta|\delta| + Y_{\delta v} \delta v^2
 \end{aligned} \tag{6.2}$$

$$\begin{aligned}
 I_z \dot{r} + mx_G(\dot{v} + ur) &= N_o + N_{o\eta}(\eta - 1) + N_{\dot{v}} \dot{v} \\
 &+ N_{\dot{r}} \dot{r} + [N_v + N_{v\eta}(\eta - 1)]v \\
 &+ [N_r + N_{r\eta}(\eta - 1)]r \\
 &+ [N_{v|v|} + N_{v|v|\eta}(\eta - 1)]v|v| \\
 &+ [N_{r|r|} + N_{r|r|\eta}(\eta - 1)]r|r| \\
 &+ N_{vrr}vr^2 + N_{r|v|}r|v| \\
 &+ [N_{\delta} + N_{\delta\eta}(\eta - 1)]\delta \\
 &+ N_{\delta|\delta|}\delta|\delta| + N_{\delta v} \delta v^2
 \end{aligned} \tag{6.3}$$

where (Resistance) and (Thrust) are measured from the resistance test and propeller open water and self propulsion test.

KRISO has conducted HPMM tests using a model ship with a length of 6.5 m in the towing tank whose dimensions are 200 m × 16 m × 7 m. All the tests were carried out with fully appended model and with the propeller operating at the ship propulsion point.

Test programs are summarized in Table 6.1 and Table 6.2. Hydrodynamic coefficients of KRISO are summarized in Table 6.3. Here, all the force coefficients are taken with the origin at the ship center of gravity.

Table 6.1 Static Test Program of KRISO.

Type	Drift Angle (deg)	Rudder Angle (deg)	Model Speed (m/s)	η
Speed & Rudder	0	0,±5,±10,15,20,25,30,35	0.509	1.0
	0	0,±5,±10,15,20,25,30,35	0.364	1.4
	0	0,±5,±10,15,20,25,30,35	0.255	2.0
	0	0,±10,20,30	0.364	1.0
	0	0,±10,20,30	0.364	0.0
	0	0,±10,20,30	0.364	-1.0
	0	0,±10,20,30	0.364	-2.0
Static Drift	0,±2,±4,6,8,12,16,24	0	0.509	1.0
	0,±2,±4,6,8,12,16,24	0	0.509	0.0
	0,±2,±4,6,8,12,16,24	0	0.364	1.4
	0,±2,±4,6,8,12,16,24	0	0.255	2.0
	2	0,±10,20,30	0.509	1.0
Drift & Rudder	4	0,±10,20,30	0.509	1.0
	8	0,±10,20,30	0.509	1.0
	12	0,±10,20,30	0.509	1.0
	12	0,±10,20,30	0.509	1.0

Table 6.2 Dynamic Test Program of KRISO.

Type	Drift Angle (deg)	Rudder Angle (deg)	Model Speed (m/s)	η
Speed & Rudder	0	0,±5,±10,15,20,25,30,35	0.509	1.0
	0	0,±5,±10,15,20,25,30,35	0.364	1.4
	0	0,±5,±10,15,20,25,30,35	0.255	2.0
	0	0,±10,20,30	0.364	1.0
	0	0,±10,20,30	0.364	0.0
	0	0,±10,20,30	0.364	-1.0
	0	0,±10,20,30	0.364	-2.0
Static Drift	0,±2,±4,6,8,12,16,24	0	0.509	1.0
	0,±2,±4,6,8,12,16,24	0	0.509	0.0
	0,±2,±4,6,8,12,16,24	0	0.364	1.4
	0,±2,±4,6,8,12,16,24	0	0.255	2.0
	2	0,±10,20,30	0.509	1.0
Drift & Rudder	4	0,±10,20,30	0.509	1.0
	8	0,±10,20,30	0.509	1.0
	12	0,±10,20,30	0.509	1.0
	12	0,±10,20,30	0.509	1.0

Table 6.3 Hydrodynamic coefficients of KRISO.

Coefficient	Value×10 ⁵	Coefficient	Value×10 ⁵	Coefficient	Value×10 ⁵
$X_{\dot{u}}'$	-138.5	$Y_{\dot{v}}'$	-1423.5	$N_{\dot{v}}'$	-29.1
		$Y_{\dot{r}}'$	39.7	$N_{\dot{r}}'$	-47.5
X_{vv}'	0.	Y_v'	-1930.9	N_v'	-761.2
		$Y_{v v}'$	-4368.1	$N_{v v}'$	118.2
X_{rr}'	133.1	Y_r'	561.4	N_r'	-322.0
X_{vr}'	1530.1	$Y_{r r}'$	206.5	$N_{r r}'$	-113.6
$X_{\delta\delta}'$	-134.0	Y_{δ}'	326.7	N_{δ}'	-147.6
$X_{v\delta}'$	-148.6	$Y_{\delta \delta}'$	0.	$N_{\delta \delta}'$	0.
		Y_{vrr}'	-3428.2	N_{vrr}'	338.2
		$Y_{r v}'$	321.8	$N_{r v}'$	-361.7
		$Y_{\delta vv}'$	-2281.3	$N_{\delta vv}'$	-109.9
		Y_o'	2.0	N_o'	-1.0
$X_{vv\eta}'$	0.	$Y_{v\eta}'$	-349.2	$N_{v\eta}'$	-28.7
		$Y_{v v \eta}'$	0.	$N_{v v \eta}'$	24.1
$X_{rr\eta}'$	0.	$Y_{r\eta}'$	54.7	$N_{r\eta}'$	-9.6
		$Y_{r r \eta}'$	0.	$N_{r r \eta}'$	0.
$X_{\delta\delta\eta}'$	-158.7	$Y_{\delta\eta}'$	411.4	$N_{\delta\eta}'$	-163.7
		$Y_{o\eta}'$	2.0	$N_{o\eta}'$	-1.0

HYDRONAUTICS

The mathematical model of Hydronautics are as follows (Hydronautics, 1980).

$$\begin{aligned}
 m(\ddot{u} - vr - x_G r^2) &= \frac{\rho}{2} L^3 \\
 [X_{\dot{u}}' \dot{u} + (X_{vr}' |\cos \beta| - X_{\dot{u}}' |\sin \beta|) vr] \\
 &+ \frac{\rho}{2} L^4 [X_{rr}' r^2] \\
 &+ \frac{\rho}{2} L^2 [X_{vv}' + X_{v\eta}' (\eta - 1)] v^2 \\
 &+ \frac{\rho}{2} L^2 u^2 [a_i + b_i \eta + c_i \eta^2] \\
 &+ \frac{\rho}{2} L^2 [u_p^2 X_{RUD}' \delta^2]
 \end{aligned} \quad (6.4)$$

$$\begin{aligned}
 m(\dot{v} + ur + x_G \dot{r}) &= \frac{\rho}{2} L^4 [Y_{\dot{r}}' \dot{r} + Y_{r|r}' r |r|] \\
 &+ \frac{\rho}{2} L^3 [Y_{\dot{v}}' \dot{v} + Y_r' ur + Y_{r\eta}' ur (\eta - 1)] \\
 &+ \frac{\rho}{2} L^2 [Y_{v|v}' v |v| \\
 &+ Y_{v\eta}' uv (\eta - 1) + Y_{v|v|\eta}' v |v| (\eta - 1)] \\
 &+ \frac{\rho}{2} L^4 (Y_{vr}' vr^2 / U) + \frac{\rho}{2} L^2 [u_p^2 (Y_{RUD}' \delta)] \\
 &+ \frac{\rho}{2} L^2 [w_p^2 Y_*']
 \end{aligned} \quad (6.5)$$

$$\begin{aligned}
 I_z \dot{r} + mx_G (\dot{v} - ur) &= \frac{\rho}{2} L^4 [N_{\dot{v}}' \dot{v}] \\
 &+ \frac{\rho}{2} L^5 [N_{\dot{r}}' \dot{r} + N_{r|r}' r |r| \\
 &+ \{1 + 2(1 - \tanh \frac{2u}{rL})\}] \\
 &+ \frac{\rho}{2} L^4 [N_r' ur + N_{r\eta}' ur (\eta - 1) + N_{v|r}' v |r|] \\
 &+ \frac{\rho}{2} L^5 [N_{vr}' vr^2 / U_R] \\
 &+ \frac{\rho}{2} L^3 [N_v' uv + N_{v|v}' v |v| + N_{v\eta}' uv (\eta - 1)] \\
 &+ \frac{\rho}{2} L^3 [N_{v|v|\eta}' v |v| (\eta - 1)] \\
 &+ \frac{\rho}{2} L^3 [u_p^2 (N_{RUD}' \delta)] + \frac{\rho}{2} L^3 [w_p^2 N_*']
 \end{aligned} \quad (6.6)$$

Hydronautics conducted HPMM tests using a model ship with a length of about 24 ft in the towing tank whose dimension is 128 m × 7.6 m × 3.9 m. All the tests were carried out with fully appended model and with the propeller operating at the ship propulsion point.

Hydronautics have carried out HPMM tests at three depths. But, only the data at deep water will be shown here. Test programs and hydrodynamic coefficients are summarized in Tables 6.4, 6.5 and in Table 6.6 respectively. Here, all the force coefficients are defined at the ship center of gravity.

Table 6.4 Static Test Program of Hydro-nautics.

Type of Test	Drift Angle (deg)	Rudder Angle (deg)	Model Speed (m/s)	η
Propulsion	0	0	0.557, 0.944	1.0
Static Drift	- 2,0,2,4, 6,8,12, 16,20	0	0.557, 0.944	0, 1.0, 2.0
Static Rudder	0	-5,5,10,15, 20,25,30,35	0	$\pm\infty$
Rudder and Drift	2,4,6,8, 12,16, 20	-35,-30,-25, -20,-15,-10, -5,5,10,15, 20,25,30,35	0.944	1.0

Table 6.5 Dynamic Test Program of Hydro-nautics.

Type of Test	Drift Angle (deg)	Rudder Angle (deg)	Model Speed (m/s)	η
Propulsion	0	0	0.557, 0.944	1.0
Static Drift	- 2,0,2,4, 6,8,12, 16,20	0	0.557, 0.944	0, 1.0, 2.0
Static Rudder	0	-5,5,10,15, 20,25,30,35	0	$\pm\infty$
Rudder and Drift	2,4,6,8, 12,16, 20	-35,-30,-25, -20,-15,-10, -5,5,10,15, 20,25,30,35	0.944	1.0

Table 6.6 Hydrodynamic Coefficients of Hydronautics.

Coefficient	Value	Coefficient	Value	Coefficient	Value
$X_{\dot{u}}'$	-0.00105	$N_{\dot{v}}'$	-0.00025	a_1	-0.0005844
X_{vr}'	0.0417	$N_{\dot{r}}'$	-0.00091	b_1	-0.0006599
X_{vv}'	0.0035	N_r'	-0.00353	c_1	0.001244
X'_{rr}	0.0003	$N_{r r}'$	-0.00069	a_2	-0.00085
$X_{\delta\delta}'$	-0.00135	N_v'	-0.007867	b_2	0.000138
$X_{vv\eta}'$	0.0021	$N_{v v}'$	0.0	c_2	0.000712
$Y_{\dot{v}}'$	-0.001746	$N_{r\eta}'$	-0.00028	a_3	-0.00085
$Y_{\dot{r}}'$	-0.00071	$N_{v\eta}'$	0.000505	b_3	-0.00002984
Y_r'	0.00595	N_{vr2}	0.003571	c_3	-0.0009475
$Y_{r r}'$	0.0023	N_*'	0.0	a_4	-0.0007343
Y_v'	-0.02048	$N_{\delta'}$	-0.001985	b_4	0.0002685
$Y_{v v}$	-0.03377	$N'_{\delta v}$	0.0	c_4	-0.0007766
$Y_{r\eta}'$	0.00060	$N'_{r v}$	-0.0034	d	0.33
$Y_{v\eta}'$	-0.00105			e	0.32
$Y_{vv\eta}'$	0.0			f	0.077
Y_{vrr}'	-0.0156	$Y'_{r v}$	0.0075	a_w	0.0
Y_*'	0.0			b_w	0.42
Y_{δ}'	0.003953	$Y_{\delta v}$	0.0	c_w	0.10

Table 6.7 Hydrodynamic Coefficients by SNU.

Coefficient	Value	Coefficient	Value	Coefficient	Value
$X_{\dot{u}}' - m'$	-0.021170	$Y_{\dot{v}}' - m'$	-0.033162	$N_{\dot{v}}'$	0.000127
		$Y_{\dot{r}}'$	-0.000638	$N_{\dot{r}}' - I_z'$	-0.001738
X_{vv}'	0.002127	Y_v'	-0.24418	N_v'	-0.007665
		Y_{vv}'	0.095876	N_{vv}'	-0.004756
X_{rr}'	-0.002770	$Y_r' - m'$	-0.011914	N_r'	-0.003774
		Y_{rr}'	-0.010450	N_{rr}'	-0.000594
$X_{vr}' + m'$	0.028172	Y_{vrr}'	0.024019	N_{vrr}'	-0.021079
X_{vrr}'	0.033843	Y_{vrr}'	-0.010450	N_{vrr}'	0.002357
X_{ee}'	-0.001497	Y_{θ}'	0.005675	N_{θ}'	0.000193
		Y_{δ}'	0.003908	N_{δ}'	-0.001745
		Y_{eee}'	0.000519	N_{eee}'	-0.000026

SNU

The mathematical model of SNU are as follows (Rhee, Key. P., et al., 1993).

$$m(\ddot{u} - vr) = \frac{\rho}{2} L^3 [X_{\dot{u}}' \dot{u} + X_{vr}' vr] + \frac{\rho}{2} L^2 [X_{vv}' v^2] + \frac{\rho}{2} L^4 [X_{rr}' r^2 + X_{vvr}' v^2 r^2 / U^2] + \frac{\rho}{2} L^2 c^2 [X_{ee}' e^2] + (Thrust) - (Resistance) \quad (6.10)$$

$$m(\dot{v} + ur) = \frac{\rho}{2} L^4 [Y_{\dot{r}}' \dot{r}] + \frac{\rho}{2} L^3 [Y_{\dot{v}}' \dot{v}] + \frac{\rho}{2} L^2 U [Y_{v'}' v] + \frac{\rho}{2} L^2 / U [Y_{vv}' v^3] + \frac{\rho}{2} L^3 U [Y_{r'}' r] + \frac{\rho}{2} L^5 / U [Y_{rrr}' r^3] + \frac{\rho}{2} L^3 / U [Y_{vvr}' v^2 r] + \frac{\rho}{2} L^4 / U [Y_{vrr}' vr^2] + \frac{\rho}{2} L^2 [Y_o' (U_{A\infty} / 2)^2] + \frac{\rho}{2} L^2 [Y_{\delta}' \delta \{-(c - c_0)(v - rL/2) + c^2 \delta\}] + \frac{\rho}{2} L^2 c^2 [Y_{eee}' e^3] \quad (6.11)$$

$$I_z \dot{r} = \frac{\rho}{2} L^5 [N_{\dot{r}}' \dot{r}] + \frac{\rho}{2} L^4 N_{\dot{v}}' \dot{v} + \frac{\rho}{2} L^3 U [N_{v'}' v] + \frac{\rho}{2} L^3 / U [N_{vv}' v^3] + \frac{\rho}{2} L^4 U [N_{r'}' r] + \frac{\rho}{2} L^6 / U [N_{rrr}' r^3] + \frac{\rho}{2} L^4 / U [N_{vvr}' v^2 r] + \frac{\rho}{2} L^5 / U [N_{vrr}' vr^2] + \frac{\rho}{2} L^3 [N_o' (U_{A\infty} / 2)^2] + \frac{\rho}{2} L^3 c^2 [N_{eee}' e^3] + \frac{\rho}{2} L^3 [N_{\delta}' \delta \{-(c - c_0)(v - \frac{rL}{2}) + c^2 \delta\}] \quad (6.12)$$

where

$$e = \delta - \tan^{-1}[(v - rL/2)/c]$$

$U_{A\infty}$; propeller induced velocity far down stream

$$= -(1 - \omega)u + \sqrt{(1 - \omega)^2 u^2 + 8K_T (nD)^2 / \pi}$$

$$c = \sqrt{R_{pr} \{(1 - \omega)u + kU_{A\infty}\}^2 + (1 - R_{pr})(1 - \omega)^2 u^2}$$

c_0 ; propeller induced velocity far down stream

D ; propeller diameter

$$R_{pr} = A_p / A_r$$

A_r ; projected area of rudder

A_p ; projected area of rudder in propeller race

ω ; wake fraction

K_T ; propeller thrust coefficient

$$k = U_A / U_{A\infty}$$

U_A ; propeller induced velocity

SNU has conducted HPMM tests using a model ship with a length of 6.5 m in the towing tank whose dimension is 200 m × 14 m × 6 m. All the tests have been carried out with fully appended model and with the propeller operating at the ship propulsion point. Test programs are almost same with that of KRISO. Hydrodynamic coefficients of SNU are summarized in Table 6.7. Here, all the force coefficients are taken with the origin at the ship center of gravity.

Comparison of mathematical model and test conditions

Mathematical models of KRISO, HSMB and SNU are basically same. Major differences are just in representing non-linear damping terms and propeller slip stream effects. SNU adopts cubic forms in representing non-linear damping terms while KRISO and HSMB adopts both square and cubic terms. KRISO models propeller slip stream effects simply just by introducing a ship propulsion ratio η . HSMB and SNU use more complicated models to represent propeller slip stream effects. They use different forms but basic idea of their modeling is same in that they model the velocity into the rudder based on propeller theory.

All three organizations carried out HPMM tests with a relatively large model and in a sufficiently large towing tank. So we can assume that all the test results have same scale effects and blockage effects. But HSMB performs test at the rather higher velocity than KRISO. So this might give some differences in force measurements due to Reynolds number effects. Test programs are very similar except a few tests. HSMB have carried out rudder and drift test for wider range of drift angles while KRISO have carried out yaw and drift test for wider range of drift angles.

6.2. Simulations

Using the mathematical models and hydrodynamic coefficients of three organizations described in the previous section, simulations of maneuvering have been made for an *Esso Osaka* tanker and the results are compared with trial data.

The results of simulation for 35 degree starboard and port turning are shown in Figures 6.1÷6.8. The agreement between trials and simulations by three models is good. There are some differences in yaw rate at the early stage of turning where turning rate has a peak value. Simulation by HSMB predicts higher yaw rate than the trial data but simulations by KRISO and SNU underpredict. Simulation by HSMB shows higher yaw rate all the time. HSMB predicts the smallest turning circle and SNU predicts the largest turning circle.

Predicted drift angles show very large differences. SNU predicts final drift angles as 24 degrees but KRISO as 12 degree. At present, it is not certain which is better prediction. Although the trial data of drift angles are shown in the figures, they are too contaminated by current to refer.

The results of simulation for 10°/10° and 20°/20° zigzag maneuver are shown in Figures 6.9÷6.16. Generally simulations by three models show good agreements with trial data. Overshoot angles are well predicted although simulation predicts a little time lagged motion. HSMB predicts much slower drop of forward speed than trial data. But the original simulation results made by HSMB shows much closer results with trial data (Barr, 1993). These differences seem to be errors in reproducing the simulations done in this study. Contrast to turning, three models predict drift angles not so different.

To relate predicted motions with hydrodynamic coefficients, predicted forces during maneuvering motions are examined. Figure 6.17 and Figure 6.18 show typical range of motion variables during turning and zigzag

maneuvers respectively. A ship experiences the largest yaw rate and drift angle at the indicated stages shown in these figures. Prediction of hydrodynamic forces at these stages would affect the prediction of maneuvering motions critically. The largest motion can be observed in the steady stage of 35 degree turning where the speed drop ratio, the drift angle and non-dimensional yaw velocity are 0.35, 18 degree and 0.9 respectively. In the zigzag maneuver, the largest motion can be observed at the second phase of 20°/20° zigzag maneuver.

Figures 6.19÷6.24 show the comparison of the predicted forces by three models over the range of turning and zigzag maneuver shown in Figure 6.17 and Figure 6.18. Generally the predicted yaw moments by three models show good agreements compared with side forces. Over the range of typical zigzag maneuver, three models predict almost same both side forces and yaw moments. But predicted forces show large differences over the range of turning motion. Especially, side forces show much larger differences. The large differences of drift angles seen in Figure 6.4 and Figure 6.8 are attributed to these differences.

The main cause of the difference in side forces at the large yaw rate and large drift angle is can be found in hydrodynamic coefficients, Y_{vrr} , $Y_{v|r|}$. The values of Y_{vrr} , $Y_{v|r|}$ by KRISO are -0.03428 and 0.00321 while those by HSMB are -0.0156 and 0.0075 . There can be many sources making this difference. The model test conditions of KRISO and HSMB including the size of towing tank and model, propulsion condition and test procedure are very similar. Just the test program for Yaw and Drift test shows a little difference. KRISO have carried out this test up to the drift angle of 16 degree while HSMB up to 12 degree. And HSMB carried out this test at the higher speed of 0.944 m/sec while KRISO at the lower speed of 0.504 m/sec. Analyzing method would also affect the results. But, unfortunately, all of these cannot be confirmed further at present because both raw model test data are not available.

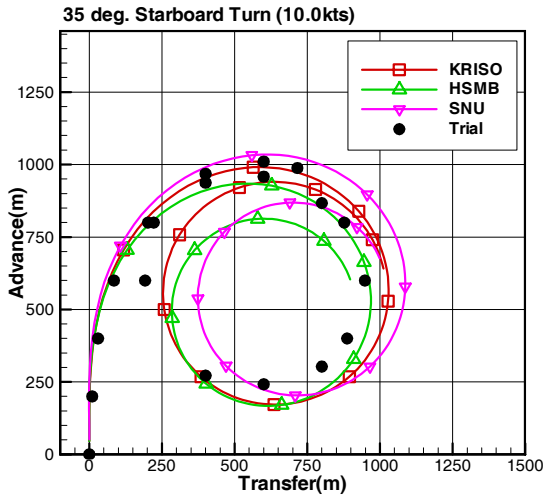


Figure 6.1 Trajectory for 35° Starboard turning (V = 10.0 kts).

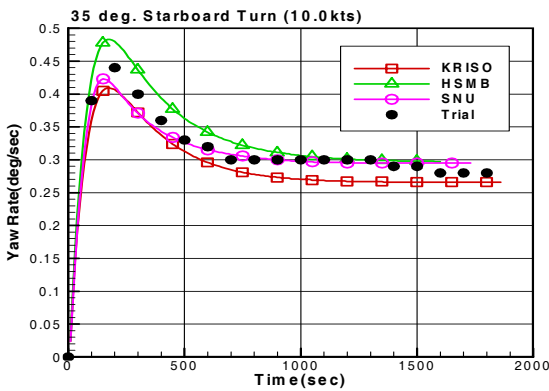


Figure 6.2 Time history of yaw rate for 35° Starboard turning (V = 10.0 kts).

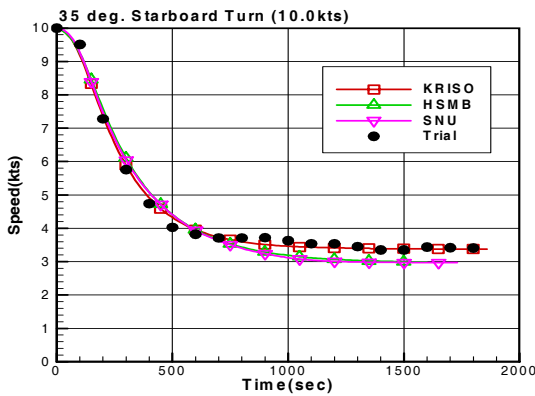


Figure 6.3 Time history of speed for 35° Starboard turning (V = 10.0 kts).

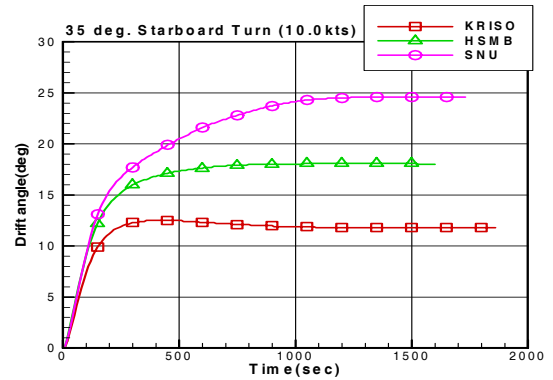


Figure 6.4 Time history of drift angle for 35° Starboard turning (V = 10.0 kts).

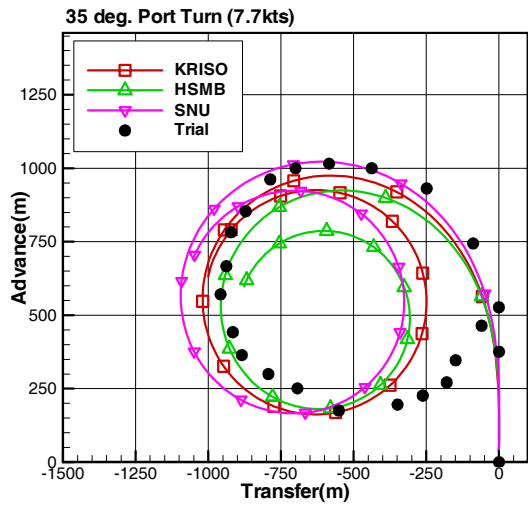


Figure 6.5 Trajectory for 35° Port turning (V = 7.7 kts).

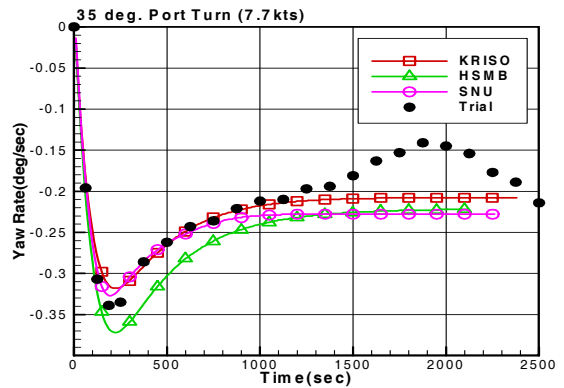


Figure 6.6 Time history of yaw rate for 35° Port turning (V = 7.7 kts).

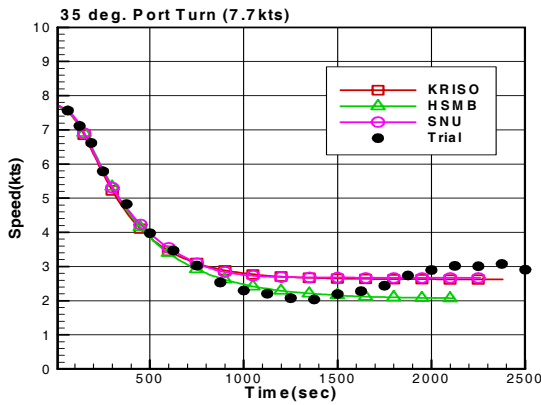


Figure 6.7 Time history of speed for 35° Port turning ($V = 7.7$ kts).

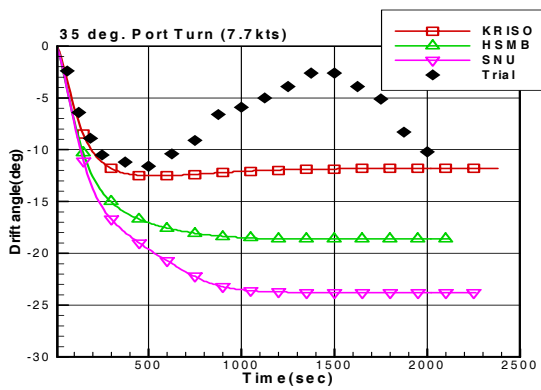


Figure 6.8 Time history of drift angles for 35° Port turning ($V = 7.7$ kts).

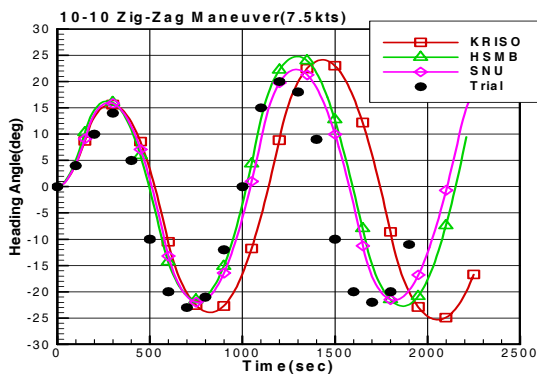


Figure 6.9 Time history of heading angles for 10°/10° Zigzag maneuver ($V = 7.5$ kts).

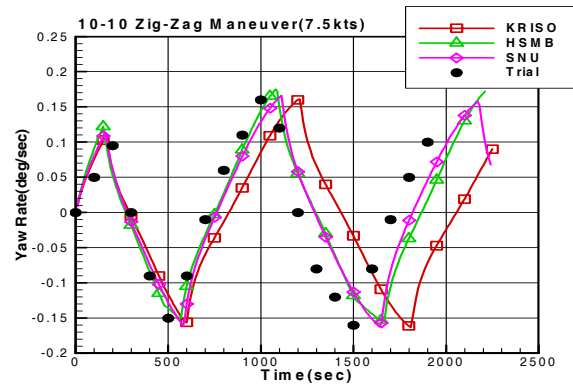


Figure 6.10 Time history of yaw rate for 10°/10° Zigzag maneuver ($V = 7.5$ kts).

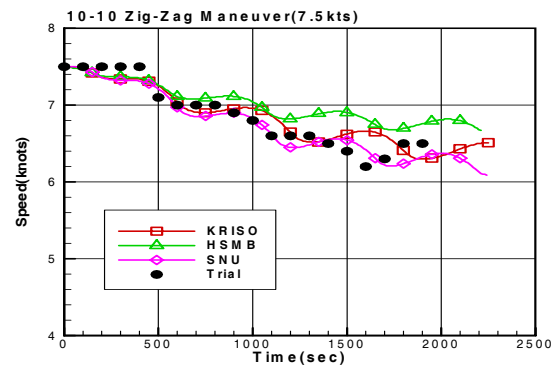


Figure 6.11 Time history of speed for 10°/10° Zigzag maneuver ($V = 7.5$ kts).

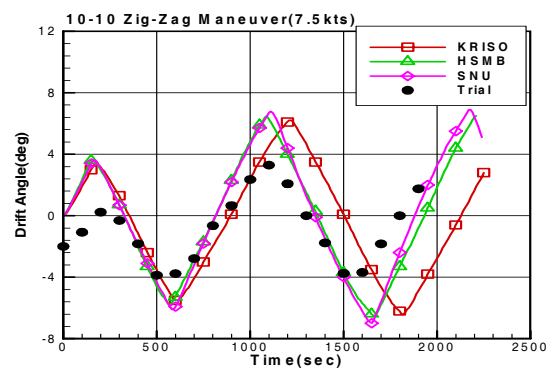


Figure 6.12 Time history of drift angles for 10°/10° Zigzag maneuver ($V = 7.5$ kts).

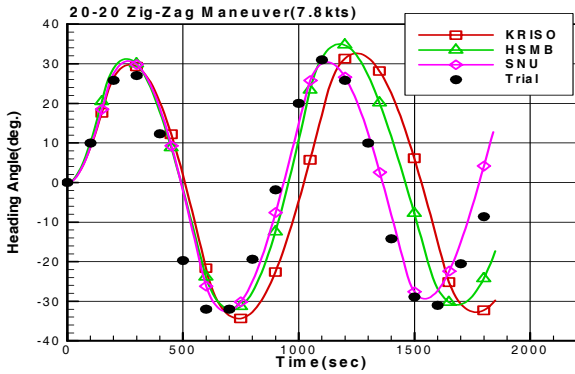


Figure 6.13 Time history of heading angles for 20°/20° Zigzag maneuver (V = 7.8 kts).

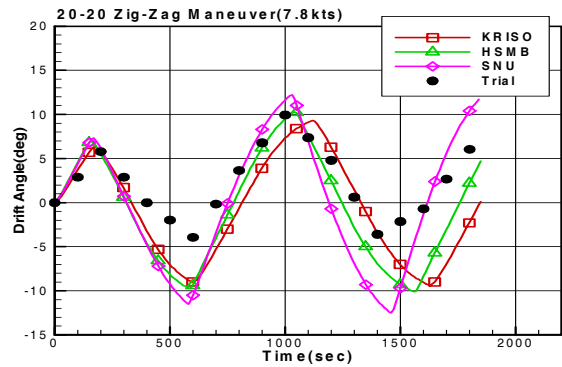


Figure 6.16 Time history of drift angles for 20°/20° Zigzag maneuver (V = 7.8 kts).

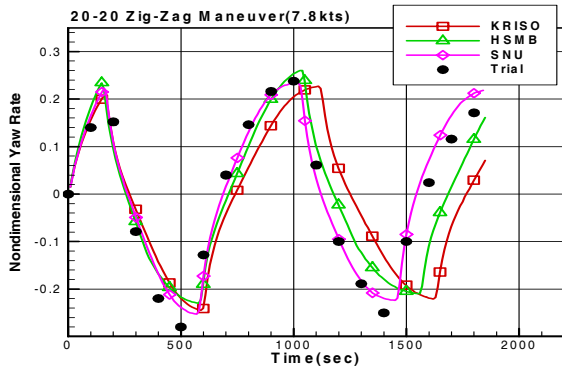


Figure 6.14 Time history of yaw rate for 20°/20° Zigzag maneuver (V = 7.8 kts).

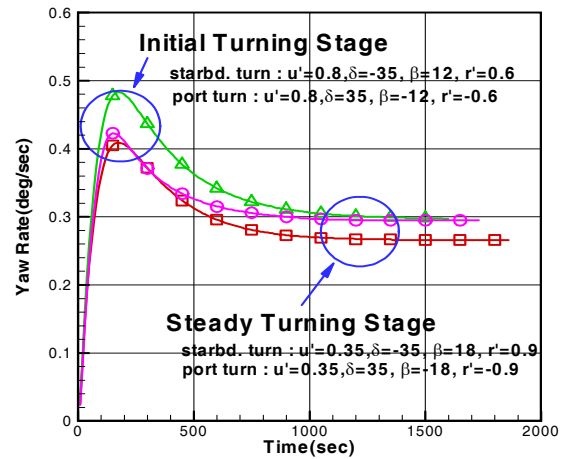


Figure 6.17 Typical values of motion variables during turning maneuver.

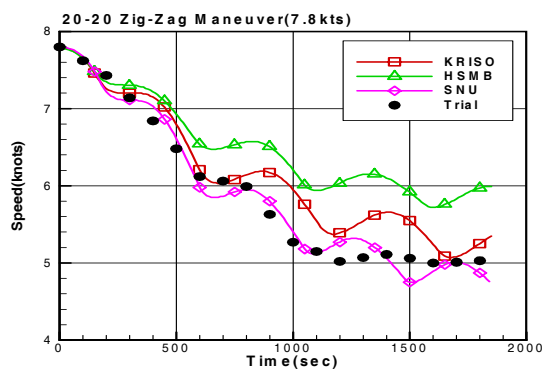


Figure 6.15 Time history of speed for 20°/20° Zigzag maneuver (V = 7.8 kts).

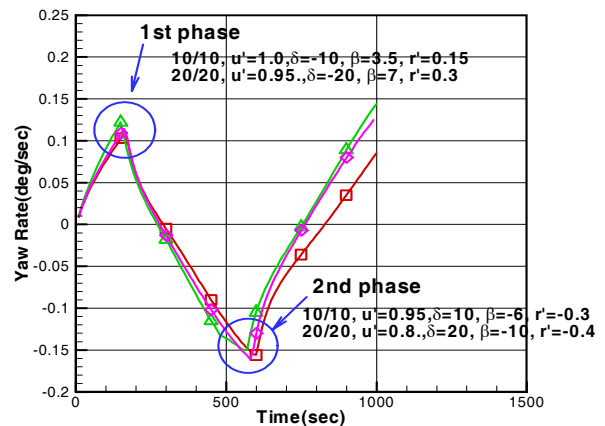


Figure 6.18 Typical values of motion variables during zigzag maneuver.

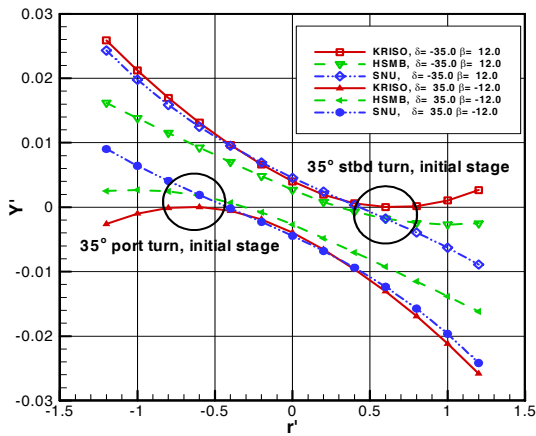


Figure 6.19 Side forces at the initial turning stage.

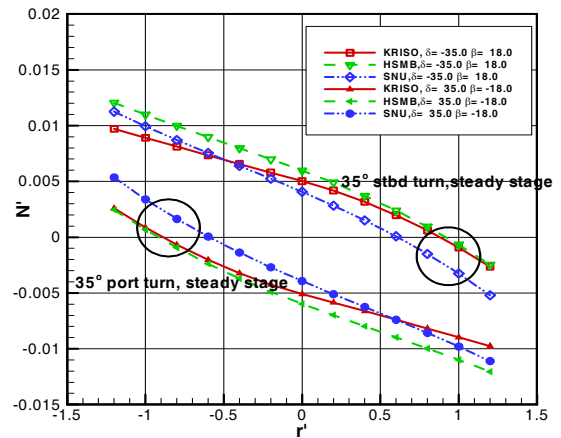


Figure 6.22 Yaw moments at the steady turning stage.

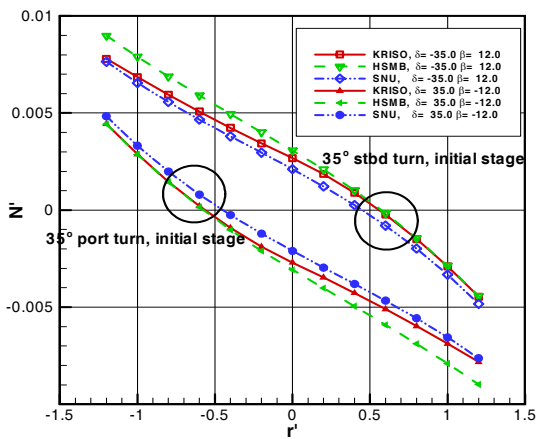


Figure 6.20 Yaw moments at the initial turning stage.

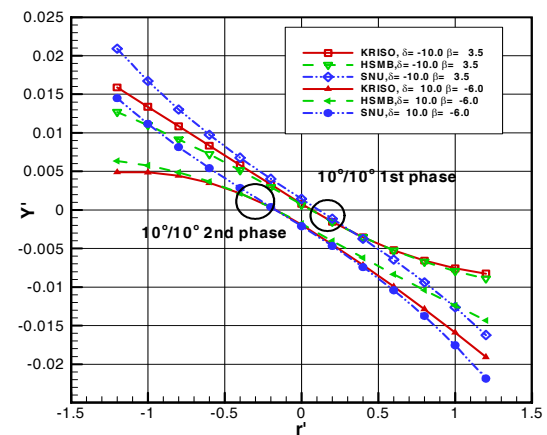


Figure 6.23 Side forces during Zigzag motions.

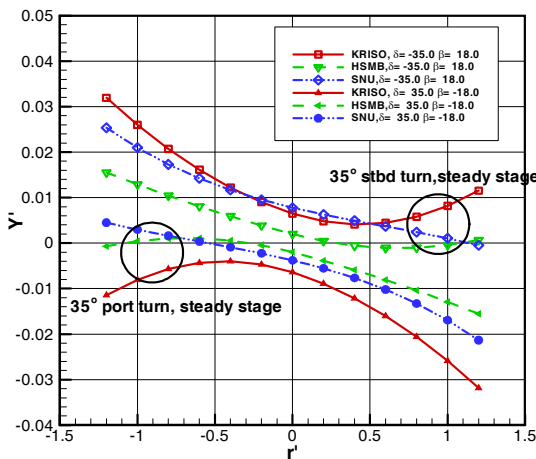


Figure 6.21 Side forces at the steady turning stage.

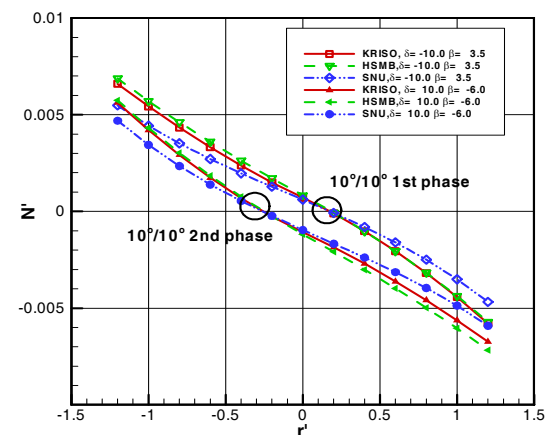


Figure 6.24 Yaw moments during Zigzag motions.

6.3. Benchmark data based on selected datasets of a whole ship model

As it is shown in the foregoing, the selected three datasets of a whole ship model gives a reasonable prediction of full maneuvering performance comparable with full scale trial data. So, their mean value of hydrodynamic coefficients can be proposed as one of benchmark data for the study of maneuvering performance of *Esso Osaka* tanker.

Since three datasets are derived based on different mathematical model and with different analyzing method, all datasets need to be reanalyzed with same method to have same expressional forms. To reanalyze three datasets, artificial PMM data are generated using programs which have been used in comparative study. The ranges of generated datasets are determined to cover the range of full scale trials. And, new hydrodynamic coefficients of three datasets are derived with same analyzing method. Table 6.8 and Table 6.9 summarize the coefficients of each dataset and mean value of them in square form and cubic form, respectively. Here, the mean values are obtained by analyzing all three datasets together. The residual errors shown in tables represent the difference of each datasets from mean value. These errors can be, therefore, thought as scattering of hydrodynamic coefficients among three datasets. Hydrodynamic coefficients concerned with static drift and pure yaw shows small scattering. But large residual errors are observed as expected.

Using mean data in Table 6.1 and Table 6.2, prediction of full scale maneuvering per-

formances are made and compared with trial data. Some other data which are not shown in tables but necessary data for simulation are adopted from datasets of KRISO. Figures 6.13-6.16 shows the results. They show reasonable prediction but a little worse results compared with ones shown in chapter 5.

6.4. Summary

Comparative simulation study of *Esso Osaka* tanker have been done using three datasets of deep water which were derived based on a mathematical model of a whole ship model. All the simulation results by three models generally show good agreements with full-scale trial data. But it is found that each model shows much different prediction of hydrodynamic forces for large yaw rate and drift angles although they predict hydrodynamic forces almost the same over the typical motion range of turning and zigzag maneuver. But large difference in predicting side forces for the large yaw rate and drift angles results in the large difference of predicting drift angles. To predict the hard maneuvering motion which may occur either from large deflection of rudder or the inherent instability of a ship, more careful experimental design and analysis of nonlinear coupling hydrodynamic coefficients are required.

As a benchmark data of hydrodynamic coefficients for whole ship model, mean data of three datasets are suggested. Simulated results using benchmark data show reasonable prediction but a little worse results compared with ones shown in chapter 5.

Table 6.8 Summary of Hydrodynamic Coefficients for Benchmark data (square form).

Coeffs.	KRISO	HSMB	SNU	Mean	Rresidual (r.m.s)	Residual (max)	Relative Error(r.m.s)
X_{vv}	0.00085	0.00348	0.00255	0.00229	0.00001	0.00017	11.5%
X_{rr}	0.00133	0.00030	-0.00286	-0.00041	0.00015	0.00245	26.8%
X_{vr}	0.03347	0.02175	0.02846	0.02789	0.00004	0.00348	6.7%
X_{dd}	-0.00135	-0.00137	-0.00038	-0.00103	0.00002	0.00025	17.7%
Y_v	-0.01953	-0.02071	-0.02279	-0.02101	0.00003	0.00073	0.5%
$Y_v v $	-0.04030	-0.03018	-0.02791	-0.03278			
Y_r	0.00562	0.00595	0.00669	0.00579	0.00003	0.00029	0.7%
$Y_r r $	0.00608	0.00230	-0.00204	0.00218			
Y_d	0.00329	0.00400	0.00382	0.00370	0.00002	0.00025	1.7%
$Y_d d $	-0.00005	-0.00003	-0.00001	-0.00003			
$Y_v r $	-0.02677	-0.01209	-0.00965	-0.01618	0.00007	0.00739	7.5%
$Y_r v $	-0.01311	0.00663	0.00599	0.00079			
N_v	-0.00763	-0.00794	-0.00884	-0.00814	0.00001	0.00017	0.4%
$N_v v $	0.00220	0.00133	0.00353	0.00236			
N_r	-0.00321	-0.00351	-0.00365	-0.00346	0.00001	0.00008	0.4%
$N_r r $	-0.00115	-0.00074	-0.00062	-0.00084			
N_d	-0.00150	-0.00198	-0.00173	-0.00173	0.00002	0.00017	2.4%
$N_d d $	0.00005	-0.00005	0.00005	0.00002			
$N_v r $	0.00275	0.00287	0.00326	0.00296	0.00002	0.00149	4.3%
$N_r v $	0.00048	-0.00290	-0.00567	-0.00268			

Table 6.9 Summary of Hydrodynamic Coefficients for Benchmark data (cubic form).

Coeffs.	KRISO	HSMB	SNU	Mean	Residual (r.m.s)	Residual (max.)	Relative Error(r.m.s)
Y_v	-0.02213	-0.02271	-0.02442	-0.02312	0.00004	0.00130	0.6%
Y_{vvv}	-0.12176	-0.08995	-0.08511	-0.09791			
Y_r	0.00608	0.00646	0.00623	0.00632	0.00004	0.00051	0.8%
Y_{rrr}	0.00189	0.00212	-0.00182	0.00188			
Y_d	0.00328	0.00399	0.00382	0.00370	0.00025	0.00002	1.7%
Y_{ddd}	-0.00005	-0.00003	-0.00003	-0.00004			
Y_{vrr}	-0.03165	-0.01367	-0.01044	-0.01867	0.00006	0.00608	4.3%
Y_{rvv}	-0.00390	0.02061	0.02172	0.00331			
N_v	-0.00750	-0.00786	-0.00766	-0.00767	0.00001	0.000169	0.4%
N_{vvv}	0.00656	0.00390	0.00929	0.00659			
N_r	-0.00347	-0.00367	-0.00378	-0.00364	0.00001	0.00014	0.5%
N_{rrr}	-0.00105	-0.00068	-0.00058	-0.00076			
N_d	-0.00149	-0.00199	-0.00172	-0.00173	0.00002	0.00017	2.4%
N_{ddd}	0.00008	-0.00005	0.00008	0.00004			
N_{vrr}	0.00338	0.00358	0.00237	0.00310	0.00002	0.00143	1.8%
N_{rvv}	0.00222	-0.00917	-0.01954	-0.00891			

7. CONCLUSION

Esso Osaka Specialist Committee in 23rd ITTC was requested to discuss the proposed data estimated by captive model test and to propose the benchmark data. Committee discussed the reasons of scattering in proposed data and decided to study the data that we can know the detail experimental and analyzing procedures. Committee made several studies based on simulation on trial and free running model test. Finally, committee proposed the benchmark data relating to 2 kinds of mathematical model.

Esso Osaka trial data include some results in shallow water condition. Committee tried to discuss the data, but we could not get sufficient data by mean of insufficient information on experiments and analyzing procedures. Finally, committee concluded to discuss the issues in deep water condition.

For benchmark data the conclusions are:

MMG model

The hydrodynamic forces proposed by different institutes show little difference from view point of comparing the scattering in results of free running model test. Therefore, we propose to use the mean data as defines herein, as a benchmark data set for hydrodynamic coefficients. We cannot make enough discussion on the forces concerning propeller and rudder because we can correct small number of them. However, as the estimated results show good agreement to the results of free running model tests, we propose the data shown in this paper as benchmark corresponding to individual mathematical model.

Whole Ship model

The mean value of hydrodynamic coefficients of three selected data sets, summarized in Table 6.8 and Table 6.9 at chapter 6, are proposed as a benchmark data for the study of maneuvering performance of *Esso Osaka* tanker for a mathematical model with whole

ship model type. On the propeller-rudder interaction model, there might be some arguments but KRISO model is proposed because it is simpler.

8. REFERENCES

- Abkowitz, M.A., 1984, "Measurement of Ship Hydrodynamic Coefficients in Maneuvering from Simple Trials During Regular Operation", Massachusetts Institute of Technology Report MIT-OE-84-1.
- Barr, R., 1993, "A Review and Comparison of Ship Maneuvering Simulation Methods", Transactions of the SNAME, Vol. 101.
- Crane, C.L., jr., 1979a, "Maneuvering Trials of the 278,000 DWT Esso Osaka in Shallow and Deep Water", Transactions of the SNAME, Vol. 87, pp. 251-283.
- Crane, C.L., Jr., 1979b, "Maneuvering Trials of the 278,000 DWT Esso Osaka in Shallow and Deep Water", Exxon International Company Report EII.4TM.79.
- Dand, I.W., and Hood, D.B., 1983 "Maneuvering Experiments Using Two Geosims of the Esso Osaka", National Maritime Institute (NMI) Report No. NMI R168.
- Hydronautics, 1980, "Model Test and Simulation Correlation Study Based on the Full Scale ESSO OSAKA Maneuvering Data", Hydronautics report No. 8007-1.
- Kim, S.Y., 1988, "Development of Maneuverability Prediction Technique", KIMM Report No. UCE.337-1082.D.
- MMG, 1985, "Prediction of Manoeuvrability of A Ship", Bulletin of the Society of Naval Architects of Japan, Published by The Society of Naval Architects of Japan.
- Rhee, K.P., Ann, S.P., Ryu, M.C., 1993, "Evaluation of Hydrodynamic Derivatives

from PMM Test by System Identification”,
Proceedings of MARSIM '93.

Roseman, D.P., Editor, 1987, “The MARAD
Systematic Series of Full-Form Ship Mod-
els”, Published by the SNAME, New
York, NY, USA.

Webster, W.C., Editor, 1992, “Shiphandling

Simulation – Application to Waterway De-
sign”, Published by the National Academy
Press, Washington, DC, USA.

Yoshimura, Y., 2001, “A study on Hydrody-
namic derivatives and interaction coeffi-
cients”, Maneuverability Prediction Group
2001, Report No. Map 8-5.

The Specialist Committee on Esso Osaka

Committee Chair: Prof. Hiroaki Kobayashi (Tokyo Univ. Mercantile Marine)

Session Chair: Dr. Georges Thiery (Bassin d'Essais des Carènes)

I. DISCUSSIONS

I.1. Discussion on the Report of the 23rd ITTC Specialist Committee on Esso Osaka: Manoeuvring in shallow water

By: Masayoshi Hirano, Mitsui Akishima Laboratory, Japan

First of all, as a member of former ITTC Manoeuvring Committee, I would like to congratulate the committee on this fine report. The committee members must have done very laborious work. I would like to make a couple of comments as follows.

1. Theoretical approach

Nowadays CFD technique has greatly been improved and practical applications are widely being attempted not only in the area of resistance and propulsion but also in other area such as manoeuvring. Such an advanced technique as CFD may be needed to develop the benchmark data with more reliability.

2. Manoeuvring in shallow water

From the view point of manoeuvring safety, ship behaviour in shallow water area is much more important than in deep water. Although there may not exist sufficient information for Esso Osaka, efforts for the benchmark in shallow water should be continued by employing such a way as theoretical approach mentioned above.

I.2. Discussion on the Report of the 23rd ITTC Specialist Committee on Esso Osaka: Selection of data sets

By: Marc Vantorre, Ghent University, Belgium, Flanders Hydraulics Research, Antwerp, Belgium

In the first place I would like to congratulate the Specialist Committee with the final results. The task, which was based on a recommendation formulated by the 22nd ITTC Manoeuvring Committee, was not an easy one, taking account of the large scatter in existing data and the fact that most tests were carried out decades ago. If time allows, I have several questions I would like to discuss, some of them directly related to the report, other being of a more general character.

Reason of data scatter

It was clear that it was an impossible task to explain the very large differences between the experimental data sets. A list of potential sources of errors was given in Chapter 3. Most of these sources are also mentioned in the Manoeuvring Captive Model Test Procedure; I would like to suggest to the next Manoeuvring Committee to check whether additional elements mentioned in the Report of the Esso Osaka Specialist Committee should be incorporated into the Procedure. I assume the Committee will agree that it would have been much easier to identify the sources of scatter if the tests had been documented in a way suggested by the Procedure; please consider

this as a strong promotion for a proper captive model test documentation system.

It would be useful to have some more detailed explanation with Figure 3.1.

Selection of data sets

In Chapter 2 it is described in which way data sets were eliminated so that only five remaining sets for both sway force and yaw moment were left. It is not clear whether the four sets of tests mentioned in Section 5.2 and in Table 5.1 have any relation with these five remaining sets; some additional information would be appreciated. If they have, some questions about the reputation of PMM yawing tests could be raised, as the four data sets in Table 5.1 are obtained by circular motion tests. Sources of scatter are more numerous in the case of PMM testing, as the number of test parameters to be selected is larger and non-stationary techniques are used for investigating quasi-steady phenomena. As the selection of the test parameters is even more important for the reliability of PMM tests, an adequate documentation of the test conditions is, especially for this type of tests, absolutely required.

It should also be mentioned that the first, “mechanical” generations of PMM systems were in some cases not able to generate a purely harmonic yaw motion without inducing drift. Moreover, only small amplitude motions could be generated with the first PMM systems, so that a sufficiently large range of yaw rates could only be obtained by increasing the PMM frequency. More recent larger amplitude PMM systems can only generate purely harmonic yawing motions if the main carriage speed can be varied during the test, and if the sway carriage is able to perform non-harmonic motions. If this is not the case, fluctuations of the longitudinal ship speed and drift will be induced, and the forces and moments caused by these parasitic motions will affect the test results.

Most of these kinematics problems can be overcome by the use of CPMC type facilities, if properly controlled.

Shallow water data

One of the primary advantages of the selection of the *Esso Osaka* for benchmark data was the availability of trial data at reduced water depth. Although I fully understand that the Committee confined its task to deep water data, this aspect being hard enough already, it can be regretted that the shallow water trial data have not been incorporated in the benchmark data. Therefore, I would like to ask the Committee’s opinion about a possible extension of its work to the shallow water case.

An analysis of available shallow water data can be expected to be still more difficult. The number of data sets is not only considerably smaller, and the scatter is certainly not less, as is illustrated in Figures I.2.1 and I.2.2. Moreover, in many cases shallow water data are only available in a format based on the deep water data. Some sources of scatter are amplified in shallow water: as an example, the effect of propulsion on lateral force and yawing moment is much more important in shallow water (Figure I.2.3).

Unified data

In order to compare the four sets of hydrodynamic hull force data in Chapter 5, unified data were calculated, i.e. instead of comparing the manoeuvring coefficients, non-dimensional forces and moments were calculated for a number of combinations of sway and yaw velocities. I fully agree that such a tabular way of presenting results is often much more useful than a set of coefficients, especially when the range of validity is not specified. Therefore, I would like to suggest promoting this methodology in either the Captive Model Test Procedure or the Validation of Simulation Models Procedure.

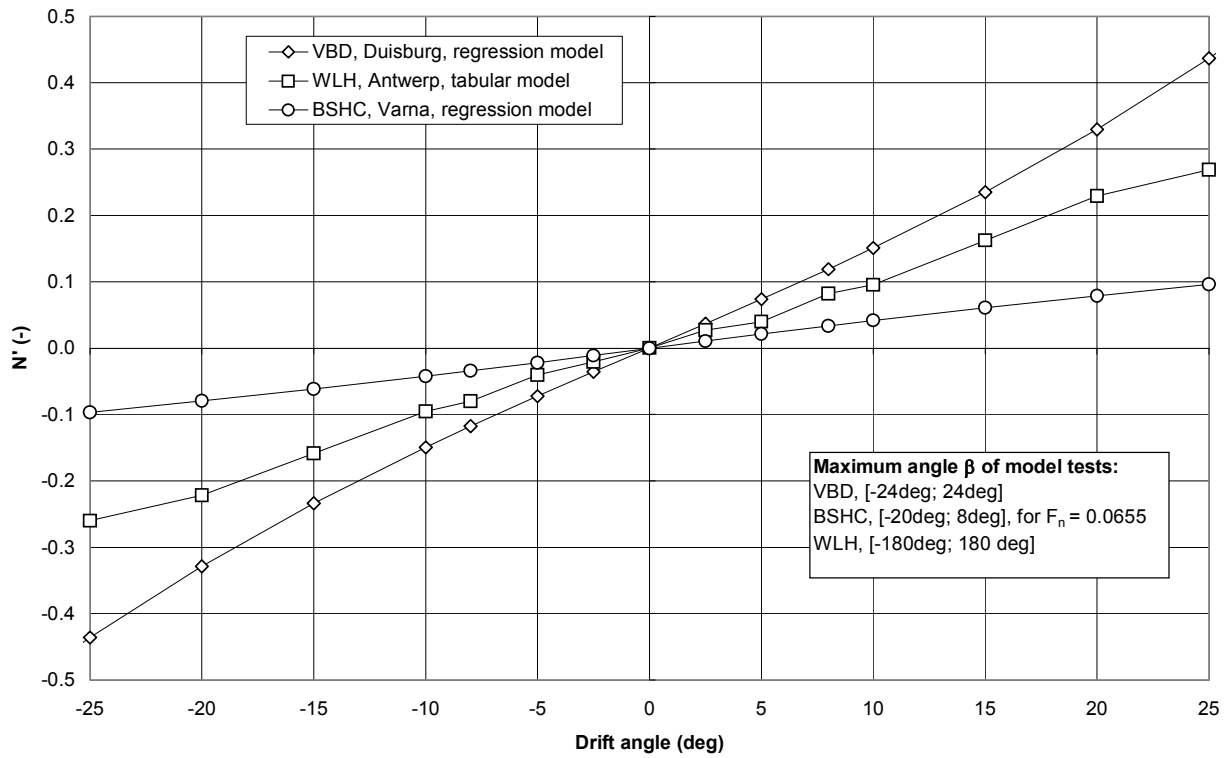
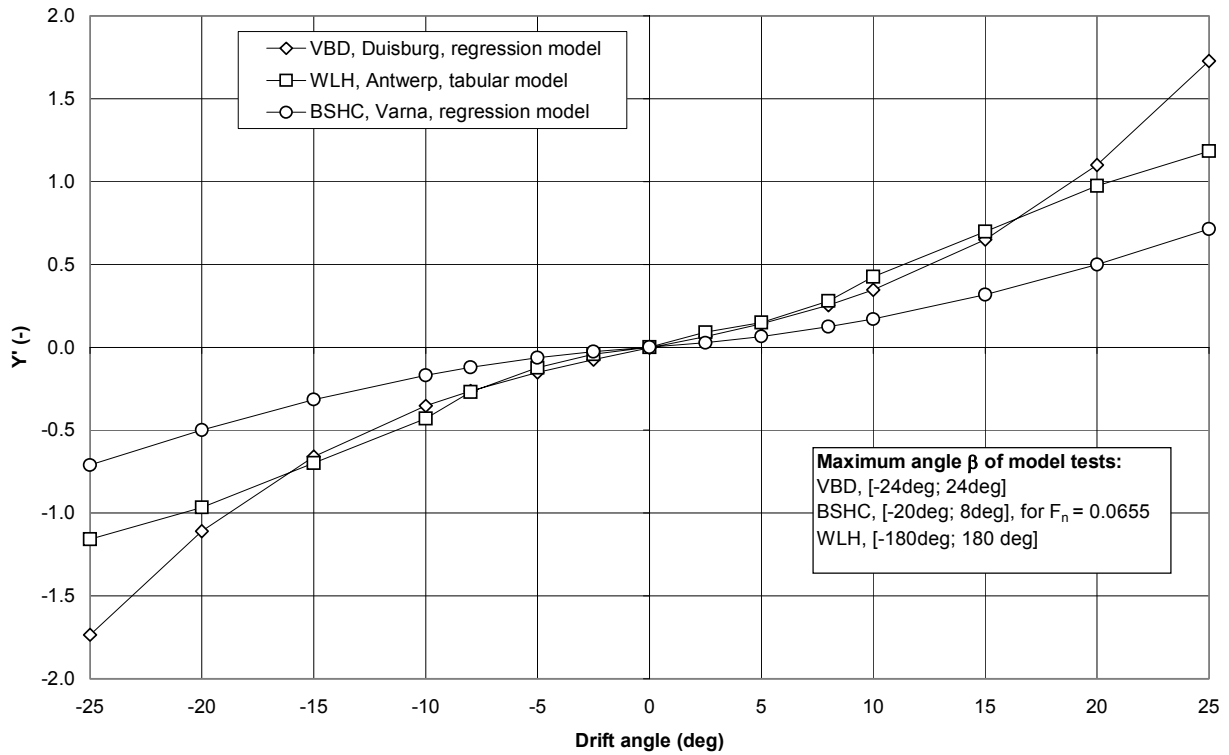


Figure I.2.1. Esso Osaka, $h/T = 1.20$: Non-dimensional lateral force and yawing moment due to drift.

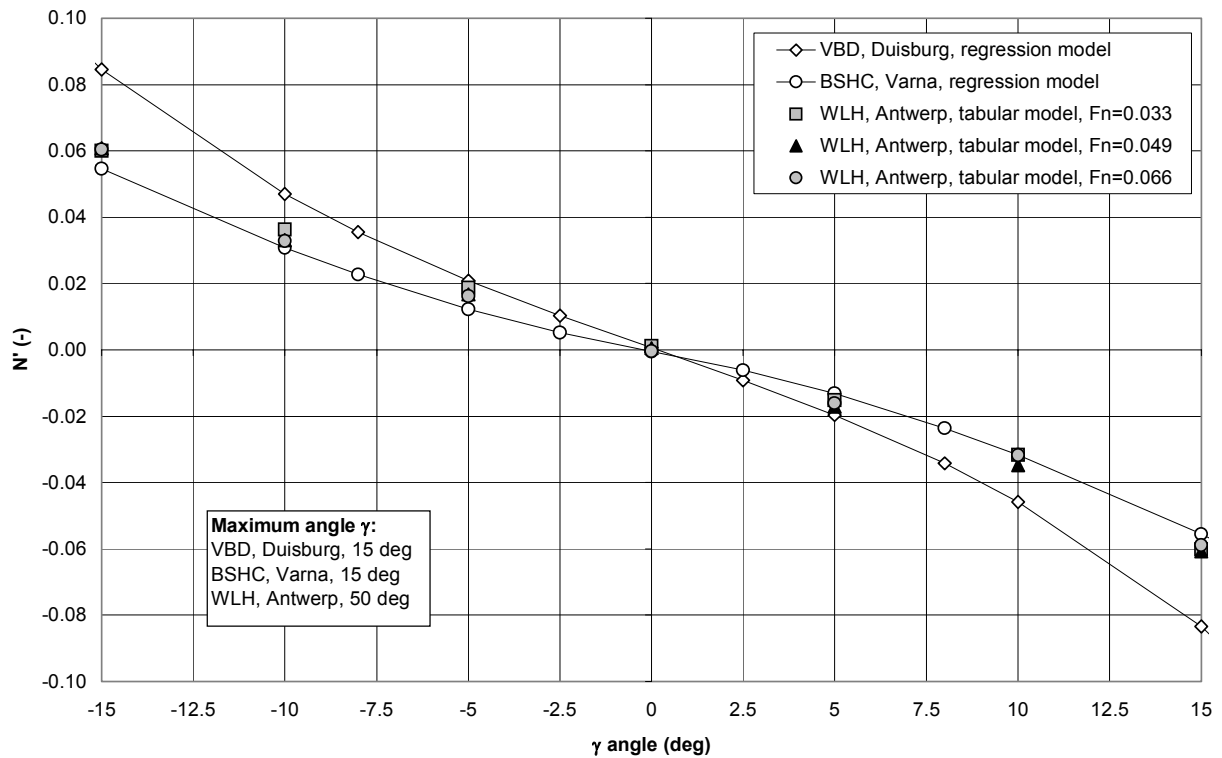
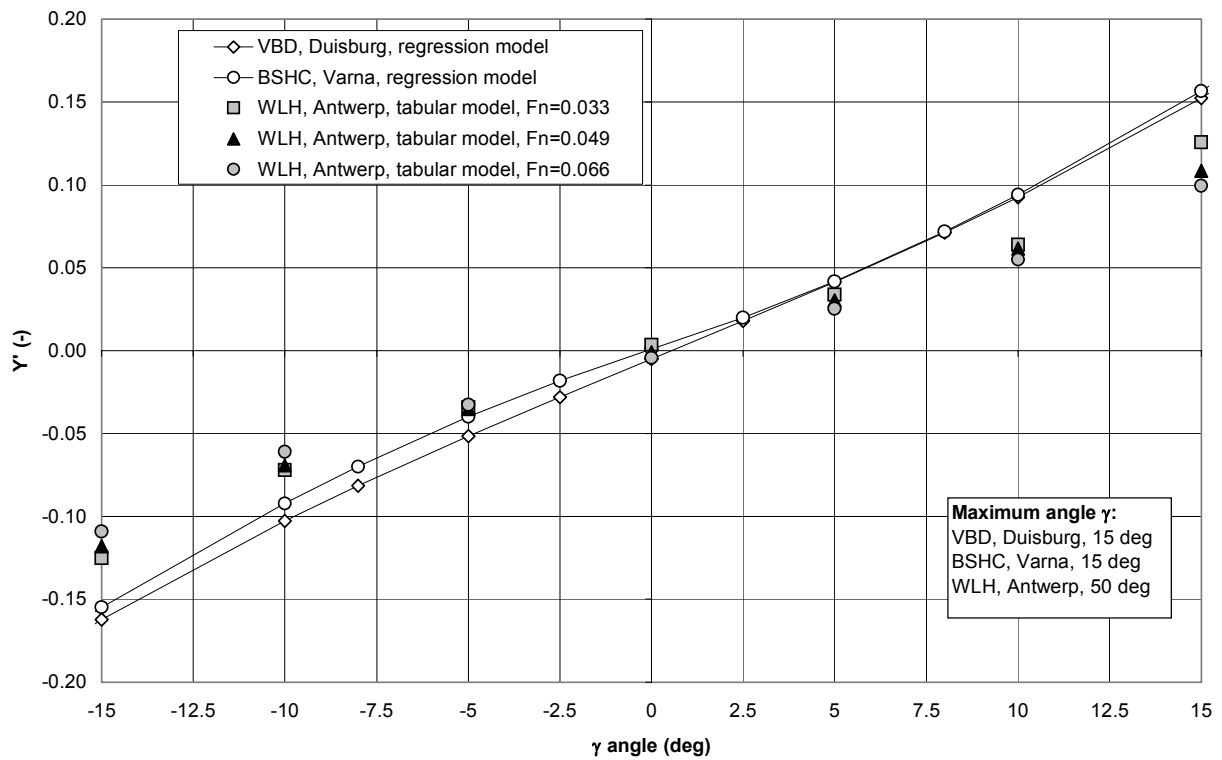


Figure I.2.2. *Esso Osaka*, $h/T = 1.20$: Non-dimensional lateral force and yawing moment due to yaw.

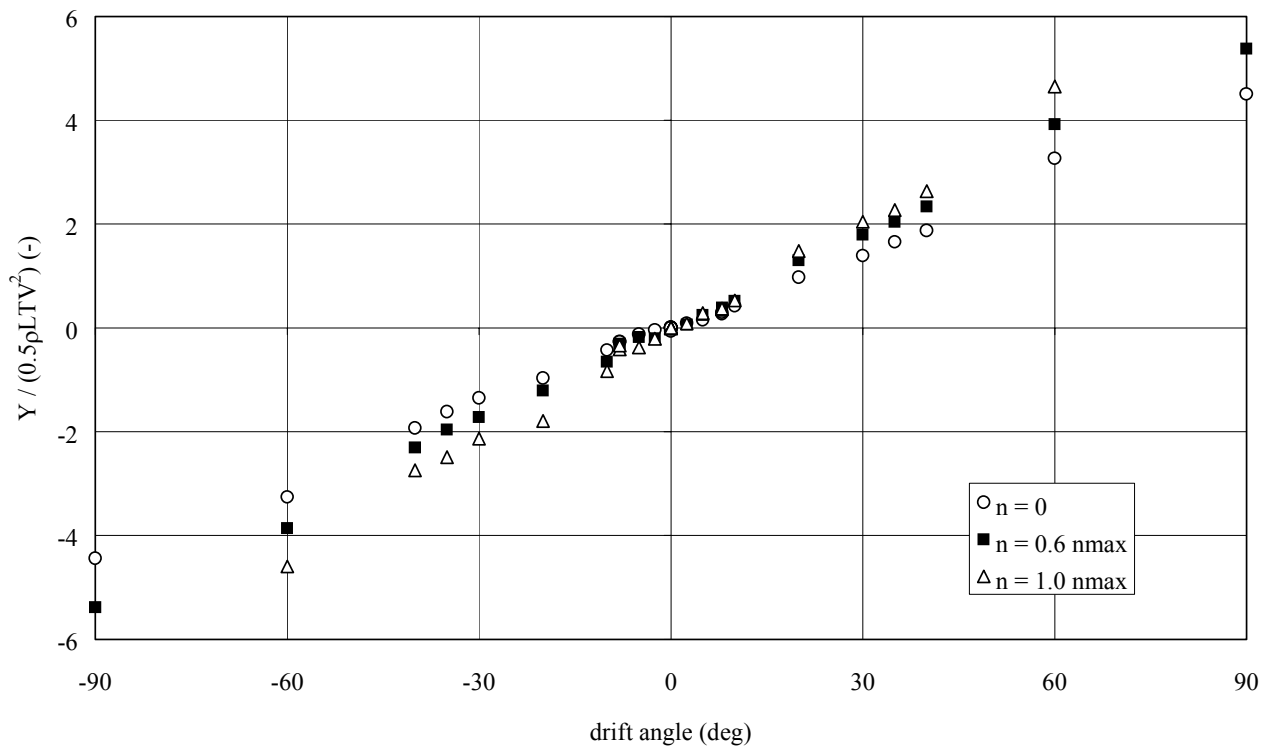


Figure I.2.3. *Esso Osaka*, $h/T = 1.20$: Non-dimensional lateral force due to drift, effect of propeller rate (Flanders Hydraulics, Antwerp).

II. COMMITTEE REPLIES

II.1. Reply of the 23rd ITTC Specialist Committee on *Esso Osaka* to M. Hirano

No reply by the Committee.

II.2. Reply of the 23rd ITTC Specialist Committee on *Esso Osaka* to M. Vantorre

No reply by the Committee.